This is a preprint, the final version is subject to change, of the American Mineralogist (MSA)
Cite as Authors (Year) Title. American Mineralogist, in press.
(DOI will not work until issue is live.) DOI: http://dx.doi.org/10.2138/am-2016-5437

Revision 3

Crystal/melt partitioning of water and other volatiles during the near-solidus melting of mantle peridotite: comparisons with non-volatile incompatible elements and implications for the generation of intraplate magmatism

JOHN. ADAM[1*], MICHAEL TURNER[1], ERIK H. HAURI[2] AND SIMON TURNER[1]

[1]Department of Earth & Planetary Sciences, Macquarie University, N.S.W. 2109, Australia

[2]Carnegie Institution of Washington, 5424 Broad Branch Road, Washington, D.C. 20005, USA

[*]Corresponding author. Tel.: +61 (02) 98504405; Email address: john.adam@mq.edu.au (John Adam)

Michael Turner Michael.turner@mq.edu.au

Simon Turner Simon.turner@mq.edu.au

Erik Hauri ehauri@ciw.edu

ABSTRACT

Concentrations of H_2O, F, Cl, C, P and S have been measured by secondary ion mass-spectrometry (SIMS) in experimentally produced peridotite phases (including clinopyroxene, orthopyroxene, olivine, garnet, amphibole and mica) and co-existing basanitic glasses. Because only two experiments produced glasses on quenching (with the melt phase in others reverting to felt-like crystallite masses) H_2O concentrations in melts were also separately determined from mass balance relationships and by assuming constant H_2O/La in melts and starting materials. The resulting values were used to calculate mineral/melt partition coefficients (D values) for H_2O (where $D_{H2O}^{crystal/melt} = \frac{mass\ fraction\ of\ H2O\ in\ crystal}{mass\ fraction\ of\ H2O\ in\ melt}$) for conditions of 1025-1190 °C and 1.0-3.5 GPa. These gave 0.0064-0.0164 for clinopyroxene, 0.0046-0.0142 for orthopyroxene, 0.0015-0.0016 for olivine, and 0.0016-0.0022 for garnet. Although less information was obtained for the other volatiles, F was found to be significantly more compatible than H_2O during peridotite melting, whereas Cl is significantly less compatible. S also has small but appreciable solubilities in amphiboles and micas, but not in pyroxenes or olivine. The solubility of C in silicate minerals appears to be negligible, although C was present in co-existing melts (~ 0.5 weight % as CO_2) and as residual graphite during experiments. The D values for H_2O in clinopyroxene and orthopyroxene are positively correlated with ^{iv}Al but negatively correlated with the H_2O concentrations of melts (when considered as weight %). These relationships are consistent with the broad trends of previously-published partitioning data. Although some of the concentration dependence can be related to cross-correlation between ^{iv}Al in pyroxenes and H_2O concentrations in melts (via the latter's control of liquidus temperatures) this relationship is too inconsistent to be a complete explanation. A concentration dependence for $D_{H2O}^{mineral/melt}$ can also be independently predicted from speciation models for H_2O in silicate melts. Thus it is likely that $D_{H2O}^{pyroxene/melt}$ is influenced by both ^{iv}Al and the absolute concentration of H_2O in melts. D_{H2O}/D_{Ce} for

clinopyroxene is inversely correlated with M2 site radii. Because the latter decrease with increasing pressure and temperature, relatively hot and/or deeply derived melts should be enriched in Ce relative to H_2O when compared to melts from cooler and shallower mantle sources. Conversely, melts from H_2O-rich settings (e.g. subduction zones) should have higher H_2O/Ce than their source rocks. When combined with previously obtained partitioning data for non-volatile elements (from the same experiments), our data are consistent with the enrichment of intraplate basalt sources in both volatile and non-volatile incompatible elements by small-degree melts derived from local mid-ocean ridge basalt sources. In this way, volatiles can be seen to play an active role (via their promotion of partial-melting and metasomatic processes) in the auto-regulation of incompatible element concentrations in the depleted upper mantle.

Key words: experiments; partitioning; basanite melts; peridotite minerals; H_2O; water; halides; carbon; sulphur; volatiles; incompatible elements; intraplate magmatism

This is a preprint, the final version is subject to change, of the American Mineralogist (MSA)
Cite as Authors (Year) Title. American Mineralogist, in press.
(DOI will not work until issue is live.) DOI: http://dx.doi.org/10.2138/am-2016-5437 12/2

INTRODUCTION

The capacity of nominally volatile-free minerals (e.g. pyroxenes, olivine and garnet) to store volatiles (e.g. H_2O and halogens) within the mantle (e.g. Wilkins and Sabine 1973; Aines and Rossman 1984; Bell and Rossman 1992; Kohn 1996; Hervig and Bell 2005) has significant implications for the Earth's deep volatile cycle. This can be linked to the ability of volatiles to promote melting and thereby regulate not only their own concentrations in the mantle, but also those of other (non-volatile) incompatible elements. Thus knowledge of how volatile and non-volatile elements partition between mantle minerals and melts is important for understanding the inter-linkage of the Earth's deep volatile cycle with the history of chemical exchange between its mantle and crust/hydrosphere. Such an understanding is pertinent to long standing debates regarding the origins of intraplate magmatism (e.g. Morgan 1971; Hofmann and White 1982; Michael 1995; Pilet et al. 2005; Putirka et al. 2007).

In this study, we take advantage of materials available from a previous experimental study (Adam and Green 2006) to examine the partitioning of H_2O, Cl, F, S and C between peridotite minerals (including clinopyroxene, orthopyroxene, olivine, garnet, amphibole and mica) and co-existing nepheline basanite melts. The analyses were conducted by secondary ion mass-spectrometry (SIMS) at the Carnegie Institution of Washington. Because the same experiments (at 1.0-3.5 GPa and 1025-1190 °C) were previously used to study non-volatile element partitioning in an intraplate magma (Adam and Green 2006), we use our data to investigate the

origins of linked volatile and non-volatile element enrichments in intraplate magmas and how these might be shaped by regional geodynamic processes.

EXPERIMENTAL AND ANALYTICAL METHODS

Starting material

The nepheline basanite (UT-70489) used in experiments is from Bow Hill in Tasmania, Australia (see Adam 1990; Adam and Green 2011). It belongs to a Cainozoic intraplate basalt province that extends discontinuously along eastern Australia from Tasmania to Cape York (see Johnson 1989). It is also notable because of the xenoliths of garnet lherzolite that it contains (Sutherland et al. 1984). The basanite has a primitive composition and may represent either a primary or near-primary partial-melt of mantle peridotite. Adam (1990) determined liquidus conditions for multiple saturation with garnet lherzolite at approximately 1200 °C and 2.7 GPa, with 4.5 weight % of dissolved H_2O and 2.0 weight % of dissolved CO_2.

High-pressure experiments

A list of experimental conditions and run products for the experiments described in this study is given in Table 1. Details of the procedures and materials used in the experiments are contained in Adam and Green (2006). In brief, the experiments were performed in end loaded piston-cylinder apparatus at Macquarie University. The starting material was a trace element enriched glass (prepared from the natural basanite and ~1.4 weight % of added trace element oxides) together with 5-10 weight % of H_2O (added with a graduated micro-syringe), contained in

graphite-lined Pt capsules. All additions were carefully monitored by weighing at each stage of capsule preparation to insure against unintended alterations to planned H_2O concentrations. Experimental conditions varied from 1.0 to 3.5 GPa and 1025 to1190 °C. Oxygen fugacities were not buffered, but are believed to be relatively low in the furnace types used [between Ni-NiO and magnetite-wustite (see discussion of Green 1976)]. Pressure and temperature tended to be positively correlated, since most experiments followed the positive slope of the basanite's liquidus. Run durations were 48 hours. To encourage the growth of large crystals, experimental temperatures were initially raised to 110 °C above final run temperatures. They were then held constant for 30 minutes before being gradually lowered over the next thirty minutes to final run temperatures.

Although none of the experiments was simultaneously saturated with more than two peridotite phases (clinopyroxene, orthopyroxene and olivine), the experiments were designed to bracket previously-identified conditions of liquidus saturation with garnet lherzolite (~ 2.7 GPa and 1200 °C). Thus for a subset of the experiments performed (1955, 1956, R80, 1948, R77) conditions approximated those of actual peridotite melting. Additional experiments were also conducted that extend the range of conditions investigated (1.0-3.5 GPa and 1025-1190 °C). These allow the effects of pressure, temperature and H_2O concentration on D values for individual minerals to be separately investigated.

Analyses of non-volatile elements

The methods used to analyse major, minor and trace element concentrations are reported in Adam and Green (2006). Major elements were analysed with a Cameca® SX50 electron

120 microprobe. Trace, minor and some major elements were analysed with a laser microprobe
121 coupled to an Agilent® 7500S ICP-MS.

122

123 **Analyses of H_2O, F, Cl, S and C**

124 The concentrations of water, F, Cl, P, S and C (as CO_2) in experimentally made minerals and
125 glasses were measured by SIMS using a Cameca 6F ion probe at the Carnegie Institution of
126 Washington. The methods employed were similar to those developed for the micro-analysis of
127 trace concentrations of volatiles in mantle minerals by Hauri et al. (2002, 2006) and Koga et al.
128 (2003). Pressure in the ion probe sample chamber was $< 6\times10^{-10}$ Torr during all analyses.
129 Background limits (typically 5-50 ppm H_2O; 1-2 ppm CO_2; < 1 ppm F and Cl) were determined
130 by the repeated analysis of synthetic forsterite located on each sample mount. Before each
131 analysis the secondary ion images of ^{12}C, $^{16}O^{1}H$, ^{19}F, ^{31}P, ^{32}S and ^{35}Cl were projected on the
132 channel plate. This helped to avoid inclusions and cracks, which appear as bright features on the
133 projected image. After each beam spot was carefully examined, the field aperture was inserted to
134 permit transmission of ions only from the central 8 μm of the 20 μm beam crater, thus avoiding
135 transmission of hydrogen ions from the edge of the sputter crater and the surface of the sample.
136 Rastering of the primary beam over a 50 μm by 50 μm area for 2 minutes was also done to
137 remove any surface contaminates prior to each analysis. The number of analyses obtained for
138 individual phases in each experiment ranged from 1 to 5, depending upon the availability of
139 suitable spots.

140 All analyses were acquired during a single session and calibrations for water in glass, olivine,
141 clinopyroxene, orthopyroxene and garnet were verified prior to the analytical session (Koga et al.

2003). Halides, C and S were calibrated using glass standards following Hauri et al. (2002). Calibration involved simple multiplication of $^{16}O^{1}H/^{30}Si$ ratios by calibration factors. The determination of these factors was done at the beginning of the analytical session and involved a comparison of $^{16}O^{1}H/^{30}Si$ ratios determined by SIMS analysis and water concentrations in glass and mineral standards that had been independently analyzed by Fourier transform infrared spectroscopy, manometry or nuclear reaction (Koga et al. 2003).

Koga et al. (2003) showed that calibration factors for micas and amphiboles are similar to those for basaltic glasses. However, they also noted that the calibration might be affected by amphibole Fe concentrations with relatively low Fe phases (< 8 weight % FeO total) having calibration factors similar to those of orthopyroxene. Our experimentally produced amphiboles and micas have relatively low Fe contents and thus (following Koga et al. 2003) we have used the calibration factor for orthopyroxene to determine H_2O concentrations.

The estimation of water and other volatiles in the melt phase

Of the eight experiments analysed by SIMS in this study, only two produced melts that transformed to a glass (Fig. 1a) on quenching (runs R79 and 1951). Consequently, only melts from these two experiments were analysed by SIMS for H_2O, F, Cl, S and CO_2. In the other six experiments, quenching of the melt phase produced a felt-like matrix of fine crystals and possible interstitial glass (Fig. 1b). H_2O concentrations for these were assessed in three different ways. The first used mass balances of major element concentrations between run products and starting compositions. This approach involved two assumptions. One is that all melts were H_2O-undersaturated (and thus H_2O was entirely dissolved in either silicate melts or crystals during

experiments). The other is that the H_2O concentrations added to starting mixes are accurately known and remained unchanged during experiments. Previously-published solubility data (Brey and Green 1977; Eggler and Burnham 1984; Carroll and Blank 1997; Jakobson 1997; Schmidt and Behrens 2008; Behrens et al. 2009) for both diopside and alkaline mafic melts indicate solubilities of approximately 10 weight % H_2O per GPa under H_2O-saturated conditions. This is consistent with our own determination of H_2O solubility (~ 28 weight %) in the molten Bow Hill basanite at 2.5 GPa (from unpublished phase equilibria and liquidus point depressions).

For most of our experiments the estimated melt-H_2O concentrations are significantly less than expected solubilities. In only one case (run 1951 with an estimated 10.7 ± 0.3 weight % of dissolved H_2O at 1.0 GPa) is H_2O-saturation likely, but this experiment was not used for the determination of any partition coefficients. The amount of H_2O added to capsules was carefully measured and checked at all stages of capsule preparation. However, H_2O loss (or gain) during experiments via the diffusion of H_2O through capsule walls is difficult to entirely preclude. Nevertheless, a number of factors mitigate against serious losses of this kind. One is that H_2O loss should result in a progressive increase in liquidus temperatures with increasing run duration, but this has not been observed for the Bow Hill composition (neither is it a problem widely reported in the experimental literature – unlike the equivalent problem of Fe-loss). In addition, the mass-balance estimates compare well with estimates based on differences between analytical totals and 100 % (i.e. the sums of all non-hydrous components in quenched melts subtracted from 100 %). Although the latter method is relatively imprecise, since it is affected by the accumulated analytical errors of multiple components, it is independent of assumed bulk H_2O concentrations during experiments. Thus we are confident that H_2O concentrations in capsules were not significantly altered during experiments.

A second method of estimating H_2O concentrations in melts was to assume that H_2O/La in melts was the same as in starting mixes [on account of both H_2O and La having very small compatibilities in the major crystal phases (see Adam and Green 2006; Hauri et al. 2006)]. The H_2O concentrations of melts could then be estimated from previously analysed La concentrations (from Adam and Green 2006). Both F and Cl were analysed in a number of glass and matrix samples by Adam and Green (2006) with the Cameca® SX50 electron microprobe at Macquarie University. For this present study, all other runs were similarly analysed using a Cameca® SX100 electron microprobe. Counting times were 20 seconds for peaks and 10 seconds for each background using a beam current of 20 nA and accelerating voltage of 15 kV. In all cases a 30 μm beam diameter was used. The standards were F-bearing topaz and chlor-apatite. ZAF corrections were performed using the method of Pouchu and Pichoir (1984).

RESULTS

The experiments produced crystals of clinopyroxene ± orthopyroxene ± olivine ± garnet ± mica ± amphibole, together with co-existing basanitic melts. A list of run products and conditions for individual experiments is given in Table 1. Minimum crystal diameters varied, but ranged up to several hundred microns and were in most cases large enough to prevent overlap by the (20 μm diameter) beam of the ion probe.

Analyses of H_2O, F, Cl, P and C (as CO_2) in individual run products are reported in Table 2, together with pressures and temperatures for each experiment. Mineral/melt D values (where $D_Z^{\text{crystal/melt}} = \frac{mass\ fraction\ of\ element\ Z\ in\ crystal}{mass\ fraction\ of\ element\ Z\ in\ melt}$) calculated from these data are shown in Table 3. Measurable concentrations of H_2O and F were found in all phases (crystals and glasses). These

concentrations are significantly above the measured backgrounds and statistical uncertainties. SIMS analyses of P (analysed concurrently with H_2O, F, Cl and C) gave concentrations that were in most cases similar to those obtained previously by laser ICP-MS (see Adam and Green 2006). Concentrations of Cl and S were simply too low in most crystals to be effectively measured, although significant concentrations were found in the glasses. The exceptions were amphibole and mica which both contained measureable concentrations of Cl and S.

There is reasonable agreement between the electron microprobe and SIMS analyses of Cl, except for one glass sample (run 1951) containing the highest measured concentration (Table 2). However, F concentrations determined by SIMS are close to double those measured by the electron microprobe. This is probably due to an overcorrection for backgrounds during electron micro-probe analyses of Fe-rich samples.

Melts

Melt H_2O concentrations estimated from mass balances and assumed H_2O/La vary from 5.6 to 16.8 weight % (Table 2). Estimates produced by the two methods are mostly within a few percent of each another on a relative basis (Table 2, Fig. 2). The exceptions are runs 1955 and R78 for which the relative differences are 18 % and 20 % respectively. Estimates from the first two methods also correlate with H_2O concentrations determined by difference (i.e. the analytical totals of all non-hydrous components subtracted from 100 %), although for the third method, the scatter of results is more pronounced (Fig. 2). The two SIMS analyses of glasses (Table 2, Fig. 2)

gave values that are 20-30 % less (on a relative basis) than determined either by mass balance or from H_2O/La.

Halide concentrations measured by both SIMS and electron microprobe [up to 0.41 weight % for F and 1.45 weight % for Cl (by electron microprobe)] reflect the high concentrations present in the starting materials. Carbon concentrations are close to 0.5 weight % (as CO_2) in both of the glasses analysed by SIMS, whereas S concentrations are 185-421 ppm (Table 2).

Clinopyroxene

Water concentrations in clinopyroxenes vary from 608 to 1390 ppm (Table 2). One sigma uncertainties (40 -150 ppm H_2O) calculated from replicate analyses are significantly larger than those attributable to counting statistics alone (8-54 ppm) but mostly within ± 20 % (relative) of average values. Calculated D values for clinopyroxene and melt ($D_{H2O}^{cpx/melt}$) vary from 0.006 to 0.016, although most are close to 0.009 (Table 3). As found in other studies (e.g. Hauri et al. 2006; Tenner et al. 2009; O'Leary et al. 2010) $D_{H2O}^{cpx/melt}$ tends to increase with increasing ^{iv}Al (Fig. 3a). But $D_{H2O}^{cpx/melt}$ also correlates negatively with H_2O concentrations in melts (Fig. 3b). When the Bow Hill data (this study) are plotted together with previously published data (Fig. 3b), the correlation between $D_{H2O}^{cpx/melt}$ and melt H_2O concentrations produces a distinctively curved trend that is initially very steep (for H_2O concentrations up to ~ 8 weight %), but then becomes increasingly shallow. Both correlations (Figs. 3a and 3b) show significant scatter.

F concentrations in the experimentally produced clinopyroxenes vary from 143 to 326 ppm (Table 2) and are positively correlated with ^{iv}Al (Fig. 4). A partition coefficient for F calculated for coexisting clinopyroxene and glass in run R79 has a value of 0.05. This is several times larger than the value determined for H_2O (0.013) in the same experiment. It falls within the range of values (0.03-0.15) previously obtained by Beyer et al. (2012) and Dalou et al. (2012) for pyroxenes and silicate melts at 1265-1445 °C and 1.2-2.5 GPa.

Orthopyroxene

Concentrations of H_2O and F in orthopyroxene are only slightly less than for coexisting clinopyroxenes and show similar relationships to ^{iv}Al and H_2O concentrations in melts (Figs. 5a and 5b).

Olivine

Olivines suitable for SIMS analysis were produced in only two experiments, R77 and R79 (at 2.0 and 1.0 GPa respectively). These have small but measureable concentrations of H_2O (94-166 ppm) and F (19-34 ppm). $D_{H2O}^{olivine/melt}$ and $D_F^{olivine/melt}$ are correspondingly low but similar for both experiments (Table 3). They plot in the mid-range of values that have been produced in similar experimental studies (e.g. Koga et al. 2003; Aubaud et al. 2004; Hauri et al. 2006; Grant et al. 2007; Tenner et al. 2009) at pressures from 1.0 to 3.0 GPa (Figs. 6a and 6b).

Garnet

Garnet was produced in only two experiments (runs 1955 and 1956). H_2O and F concentrations for these (216-352 ppm and 26-35 ppm respectively) are significantly less than for coexisting clinopyroxenes (Table 2). Measured D values for H_2O (Fig. 7) are correspondingly small (0.0022 and 0.0016) and similar to values obtained in previous experimental studies (e.g. Hauri et al. 2006; Aubaud et al. 2008; Tenner et al. 2009).

Amphibole and mica

The 1.69 weight % of H_2O in amphibole that was measured by SIMS is higher than previously estimated from structural parameters (1.40 weight %) by Adam et al. (2007), but is still consistent with some replacement of OH^- by O^{2-} at the O3 site (normally occupied by OH^-). Both amphibole and mica also contain significant F, together with small but measureable concentrations of S and Cl. S concentrations in mica are approximately double those measured for amphibole.

DISCUSSION

Analytical results

Measured H_2O concentrations in the crystals and melts from our experiments are significantly above backgrounds and statistical uncertainties (~10 ppm for most measurements). They are also

consistent with concentrations previously measured in similar phases by a variety of other techniques (e.g. Wilkins and Sabine 1973; Aines and Rossman 1984; Bell and Rossman 1992; Kohn 1996; Koga et al. 2003). Thus they are likely to represent structurally bound H_2O. SIMS analyses of P are also uniform for individual phases and comparable to those previously analysed by Laser ICP-MS (see Adam and Green 2006). Since the ICP-MS data could be filtered for cross contamination (since even minor contamination produces obvious deviations from the ideal parabolic trends of Onuma diagrams), significant inclusions of glass/matrix material during analyses of crystals can be discounted.

In the case of C, the possibility of contamination is more difficult to avoid. This is because the samples were previously carbon coated to allow them to be analysed by the electron microprobe. Although samples were subsequently re-polished to remove this coating, it is difficult to be certain that all deposited C was removed. Minor contamination can explain much of the variability in measured C concentrations for crystals (which vary by over a factor of ten). The lowest measured C concentrations are relatively uniform (~ 5 ppm) for all crystal phases, but still high when compared to values (< 1 ppm) determined by Shcheka et al. (2006) for carbon-saturated peridotite phases. These authors employed nearly pure ^{13}C to discriminate the effects of contamination, thus our lowest measured concentrations may still reflect local background values. In contrast, the ~ 0.5 weight % CO_2 measured for the two glasses (runs R79 and 1951) is likely to be real. It is similar to the solubility estimates of Holloway et al. (1992) for an anhydrous tholeiitic melt equilibrated with graphite at 1400 °C and 1.0 GPa under conditions significantly more reducing than the Ni-NiO buffer. Unfortunately, it is difficult to know how

313 closely this reflects conditions in our own experiments, since the effect of added H_2O and a more
314 SiO_2-poor melt composition on CO_2 solubility is unknown.

315 An unexpected finding from the SIMS analyses was the presence of S in the amphiboles and
316 micas. Although small, the concentrations are above measured backgrounds (< 1 ppm S).
317 Furthermore, S was not detected in any other crystal phases. It is possible that small amounts of
318 S (as S^{2-} ions) have substituted for OH^- at the O3 sites of the amphiboles and micas. This
319 possibility is given weight by the fact that S concentrations in the micas are double those in
320 amphibole (consistent with the relative proportions of OH sites in the two crystal structures). The
321 radius of six-fold coordinated S^{2-} is also similar to that of Cl^- [1.84 Å as opposed to 1.81 Å
322 (Shannon 1976)]. Since the latter is known to substitute for OH^- in amphiboles and micas (see
323 Oberti et al. 1993), it is probable that S^{2-} also has this ability.

324 As previously noted, SIMS analyses of H_2O in glasses give lower concentrations than estimated
325 from either mass balances or H_2O/La (Table 2). This may be the result of H_2O loss during
326 experiments caused by diffusion through capsule walls. But it may also reflect the difficulty of
327 quantitatively retaining high H_2O concentrations in silicate melts during quenching. The relative
328 consistency of concentrations determined from mass-balances and H_2O/La with estimates based
329 on the analytical totals of non-hydrous components (relative to 100 %) [Fig. 2] doesn't suggest
330 systematic H_2O loss during experiments. Thus we accept that the melt H_2O concentrations
331 derived from mass balances and H_2O/La are reliable and have used the latter for the calculation
332 of mineral/melt partition coefficients (Table 3).

333

334 **Controls on the partitioning of H_2O between minerals and melts**

Most of the data obtained in this study are for pyroxenes and so our discussion is largely focussed on this group. The two most evident influences on $D_{H2O}^{pyroxene/melt}$ are ^{iv}Al and the H_2O concentrations of melts (Figs. 3a-b and 5a-b). But there is significant scatter in both of these relationships, combined with a noticeable degree of cross-correlation between ^{iv}Al and melt-H_2O concentrations (Fig. 3c). Because temperature inversely correlates with melt-H_2O concentrations and most experiments also shadow the positive P/T slope of the liquidus, the influence of individual factors is difficult to isolate. But in the case of ^{iv}Al, experiments on simple systems (e.g. Stalder 2004; O'Leary et al. 2010) have independently demonstrated a strong positive influence on H_2O solubility. Thus some of the negative correlation between $D_{H2O}^{pyoxene/melt}$ and melt H_2O concentrations can be attributed to the previously mentioned cross-correlation between ^{iv}Al in pyroxenes and H_2O concentrations in melts (Fig. 3c). But the latter relationship is too inconsistent to be a complete explanation, so it remains possible that (while being influenced by ^{iv}Al) $D_{H2O}^{pyroxene/melt}$ is also governed by the activity-composition relations of H_2O in silicate melts.

We examined the role of melt-activity relations by considering two contrasting models for the solution of H_2O in silicate melts. These were the models of Burnham (1975), and Silver and Stolper (1985). The first treats hydrous silicate melts as mixtures of OH^- ions and 8-oxygen silicate melt units (based on the albite structural formula); whereas in the second, dissolved H_2O is present as both OH^- anions and molecular H_2O which mix with individual O^{2-} anions of the silicate melt. In the case of Burnham's model (1975), the very different molecular weights of the mixing units involved (17 for OH and ~ 293 for basanitic melts) result in large mole fractions for even modest additions of H_2O (considered on a weight basis). The relationship between H_2O concentrations determined as weight % and mole fractions is also strongly non-linear (Fig. 8a).

This influences the relationship between partition coefficients calculated as weight fractions (D values) and those calculated as molecular exchange K_Ds. This can be demonstrated if Burnham's (1975) model is used to independently calculate D values for a range of melt H_2O concentrations, but the molecular exchange K_D is held constant.

The exchange K_D that we considered was for the reaction:

$$^{[melt]}H^{+} + {}^{[melt]}Al^{+3} + {}^{[pyx]}Si^{+4} \leftrightarrow {}^{[pyx]}H^{+} + {}^{[iv]}Al^{+3} + {}^{[melt]}Si^{+4} \qquad (1)$$

where

$$K_D = \frac{[cpx]_{H^+} \times [iv]_{Al^{+3}} \times [melt]_{Si^{+4}}}{[melt]_{H^+} \times [melt]_{Al^{+3}} \times [iv]_{Si^{+4}}}$$

and

$^{[melt]}H^{+}$ = the mole fraction of H^{+} (equivalent to OH^{-}) in the silicate melt

$^{[iv]}Al^{cpx}$ = the mole fraction of tetrahedrally co-ordinated Al in pyroxene

$^{[iv]}Al^{melt}$ = the mole fraction of Al in the silicate melt.

$^{[pyx]}Si^{+4}$ = the mole fraction of Si in pyroxene

$^{[pyx]}H^{+}$ = the mole fraction of H^{+} (equivalent to OH^{-}) in pyroxene

$^{[melt]}Si^{+4}$ = the mole fraction of Si in the silicate melt

This reaction describes the substitution of H^{+} and Al^{+3} for Si^{+4} in pyroxenes as the result of chemical exchange between pyroxenes and co-existing melts. Although other substitutions are

possible, we assumed that it was the dominant mechanism active in our experiments. Mole fractions for pyroxenes were calculated by assuming that $^{[pyx]}H^{+}$ = H per 3 oxygens; $^{[iv]}Al^{cpx}$ = ^{iv}Al per 3 oxygens; and $^{[pyx]}Si^{+4}$ = Si per 3 oxygens. Mole fractions of H^{+} in the melt phase were calculated following Burnham's (1975) protocol and assuming that $OH^{-} = H^{+}$. Mole fractions of Al and Si were then calculated on the basis of their anhydrous mole fractions (of total cation sums) multiplied by the mole fractions of 8-oxygen melt units. When applied to the Bow Hill data, these relationships produced an average K_D of 0.0014 (range = 0.0009 to 0.0021). This was used to calculate $D_{H2O}^{cpx/melt}$ for melt H_2O concentrations from near zero to 40 weight % (but with otherwise constant melt and pyroxene compositions). The resulting D values produce a distinctively curved trend when plotted against melt H_2O concentrations (Fig. 8b). This follows both the Bow Hill data and the broad sweep of previously published results (Fig. 8b).

In the case of the solution model of Silver and Stolper (1985), the concentration dependence of D_{H2O} can be related to changes in the relative proportions of OH^{-} anions and molecular H_2O that occur as the total concentration of both species increases. This is a consequence of equilibrium between the relative concentrations of OH^{-}, H_2O and O^{2-} in melts that is described by the equilibrium constant:

$$k = \frac{[OH^{-}]^2}{[H_2O][O^{2-}]} \qquad (2)$$

where $[H_2O]$ is the mole fraction of molecular H_2O dissolved in the melt, $[O^{2-}]$ is the mole fraction of oxygen in the melt not chemically bound to H, and $[OH^{-}]$ is the mole fraction of hydroxyl within the melt.

A consequence of this relationship and a fixed value of *k* is that OH^- progressively decreases relative to molecular H_2O as the total concentration of $OH^- + H_2O$ increases (Fig. 9a). This was first demonstrated for silicate glasses by Silver et al. (1990) who used infrared spectroscopy to measure changes in the relative concentrations of molecular $H_2O + OH^-$ as the total concentration of both species increased. Although subsequent studies (Nowak and Behrens 1995; Sowerby and Keppler 1999) have shown that the ratio of OH^- anions to molecular H_2O is significantly higher in melts than compositionally equivalent glasses, molecular H_2O persists as a significant species, and equation 2 remains applicable. Consequently, we used the formulation of Sowerby and Keppler (1999) to calculated *k* for silicate melts at 1150-1350 °C and from this derived variations in $D_{H2O}^{cpx/melt}$ as a function of melt H_2O (from almost to zero to 40 weight %). It was assumed that $D_{OH}^{cpx/melt}$ remains constant (at an arbitrary value of 0.05) for all H_2O concentrations and that H_2O dissolves in pyroxenes only as OH^-. The resulting relationship (Fig. 9b) is less strongly curved than that previously calculated using Burnham's (1975) model (Fig. 8b) but still reproduces the broad trends of the experimental partitioning data. Although raising temperature increases *k* (Sowerby and Keppler 1999) its effect on $D_{H2O}^{crystal/melt}$ was found to be relatively small within the temperature range considered.

In spite of the significant differences between the two solution models considered, it is evident that key aspects of both models can be used to independently predict a concentration dependency for $D_{H2O}^{crystal/melt}$. On this basis and the trends shown in Figs. 3b and 5b, we propose that $D_{H2O}^{crystal/melt}$ for all crystal phases is significantly influenced by the activity-composition relations of H_2O in silicate melts, as well as by crystal-chemical influences. The second influence is illustrated in Figs. 8b and 9b where the concentration dependency of $D_{H2O}^{cpx/melt}$ is cross-cut by the independent influence of ^{iv}Al in pyroxenes. This is most noticeable for the data of O'Leary et

al. (2010) (who deliberately varied Al concentrations in their pyroxenes) and for melt H_2O concentrations of 6-10 weight % (where Al concentrations in pyroxenes are also highly variable). The effect of melt-H_2O concentrations is less evident for garnet and olivine than it is for pyroxenes. In the case of olivine (Fig. 6a) there is a dearth of data at intermediate H_2O concentrations so that any correlation is reliant on just two data points at the high end of the concentration range. The relationship is also complicated by a positive pressure dependence (Fig. 6b) (although this is only obvious at pressures $\geq$ 6 GPa) and by what may be inter-laboratory biases related to differences in the base-levels adopted for FTIR calibrations (since the later become critical at the very low H_2O concentrations typical of olivines). Most of the garnet data (Fig. 7) cluster at relatively low values (with $D_{H2O}^{garnet/melt} \approx 0.0025$), but data for both high and low melt H_2O concentrations are lacking so a consistent trend is difficult to define.

The behaviour of F, Cl, CO_2 and S during peridotite melting

We were unable to reliably detect Cl in pyroxenes, olivine and garnet (in spite of high melt concentrations), and only obtained limited data for the partitioning of F. Based on the lower limits of detection for Cl (1-2 ppm) during SIMS analyses of our run products, D values for Cl are typically $\leq$ 0.001 and in some cases considerably smaller. This suggests that Cl is significantly less compatible than H_2O during peridotite melting (compare results for D_{H2O} in Table 3). This relationship is supported by results from Dalou et al. (2012) in combination with our own partitioning data for H_2O and non-volatile elements. Thus Dalou et al. (2012) found that Cl partitions similarly to Th during peridotite melting, whereas in the Bow Hill experiments (this study; Adam and Green 2006) Th was significantly less compatible that H_2O.

In contrast to Cl, F is significantly more compatible than H_2O during peridotite melting. For the two experiments for which D values for F were determined in our study (runs R79 and 1950) $D_F \approx 5 \times D_{H2O}$. Comparable results were obtained by Hauri et al. (2006) for experiments on a similar basanite composition. Dalou et al. (2012) also showed that F is markedly more compatible than La during peridotite melting, whereas in our own experiments the compatibility of H_2O is either similar to or less than that of La.

Although neither S nor C is significantly retained in silicate minerals during peridotite melting, they can be held in sulphides and graphite (or diamond at high pressure). Under the conditions prevailing in our experiments, C (as CO_2) has a solubility of ~ 0.5 weight % (Table 1) and S ~ 0.15 weight % (Adam and Green, unpublished data). At low degrees of melting these limited solubilities will promote the preferential retention of C and S in solid residues. In this way they also provide a potential explanation for the apparent compatibilities of C and S in the depleted mantle (see Jambon 1994; Hirschmann and Dasgupta 2009). Without residual graphite and sulphide, however, both CO_2 and S can be expected to be highly incompatible. It may be for this reason that carbonatites, although notably enriched in incompatible elements generally, are pre-eminently enriched in C (see data of Wooley and Kempe 1989).

IMPLICATIONS

The relative partitioning of volatiles and other (non-volatile) incompatible elements during mantle melting

Studies of undegassed submarine glasses from mid-ocean-ridge and ocean island settings (e.g. Dixon et al. 1988; Michael 1995; Workman et al. 2006) have shown that the concentrations of some volatile and non-volatile elements are systematically correlated. For example, Michael (1995) found that H_2O/Ce in mid-ocean-ridge (MORB) and ocean island (OIB) magmas is 200(50), although Atlantic Ocean MORB and OIB typically have higher ratios, and some Pacific Ocean OIB have lower ratios (see also Workman et al. 2006). In some studies, H_2O has also been found to correlate better with La than Ce (e.g. Dixon et al. 1988) and also to decrease with increasing $^{87}Sr/^{86}Sr$ (Workman et al. 2006). Concentrations of Cl and Br correlate with more incompatible elements, such as K and Ba, whereas F correlates better with more compatible elements, such as P (Schilling et al. 1980; Saal et al. 2002; Workman et al. 2006). Although data for CO_2 are more limited, it has also been found to correlate with highly incompatible elements, such as Nb and Ba (Saal et al. 2002; Michael and Graham 2013). These relationships have been attributed to similar mineral/melt partition coefficients (D values) for matching volatile and non-volatile elements during magmatic differentiation of the mantle (e.g. Michael 1995; Hauri et al. 2006; Dalou et al. 2012). In this context, it is interesting to consider the relative partitioning of H_2O and light rare earths (LREE) during experiments on the Bow Hill basanite and related compositions. These show that D_{H2O}/D_{Ce} for clinopyroxene (which exerts the largest single control on peridotite/melt partitioning for H_2O and Ce) is not fixed but is instead controlled by other variables. The most evident of these is the radius of the M2 site (in which Ce and other LREE are preferentially located). Thus D_{H2O}/D_{Ce} decreases with increasing M2-O distance (from X-ray diffraction data), X_{Ca} and $^{M2}r_0^{+3}$ (see Blundy and Wood 1994) [Figs. 10a-b].

Although there is some scatter in the afore-mentioned relationships, they are consistent with the M2 site radius exerting a significant influence on D values for Ce, as well as other light rare

earths. As the M2 site shrinks, Ce (which is large relative to its M2 host site) is progressively excluded thereby raising D_{H2O}/D_{Ce} (it being assumed that D_{H2O} remains unaffected). The radius of the M2 site is itself pressure and temperature dependent, and decreases with increasing pressure and temperature. In peridotite compositions this relationship may be augmented by a positive pressure dependence of $D_{H2O}^{olivine/melt}$. Thus deeply derived and/or high temperature melts can be expected to have lower H_2O/Ce than those derived from shallower depths and/or lower temperatures. Conversely, melts from relatively cool and H_2O-rich settings (e.g. subduction zones) can be expected to concentrate H_2O more strongly than Ce. In this case the principle cause is the effect of melt H_2O concentration on D_{H2O} (see previous discussion).

Application to the problem of intraplate magma genesis

Competing models of intraplate magma genesis (e.g. Morgan 1971; Hofmann and White 1982; Dupuy et al. 1989; Michael 1995; Pilet et al. 2005; Putirka et al. 2007; Adam and Green 2011) can produce quite different inferences about the degree to which volatiles either actively or passively participate in the processes involved. Evidence for an active role can be found in an observation made by Michael (1995) who noted that H_2O/Ce is similar in MORB and OIB from the same geographic regions, yet more variable between regions. Michael (1995) suggested that this can be explained if OIB source regions are enriched in incompatible elements and volatiles by small-degree melts from local MORB sources, thereby inheriting the latter's H_2O/Ce. In this case, H_2O plays an active role in magmatism via its promotion of partial-melting and metasomatic processes.

Michael's (1995) idea can be tested by using mineral/melt partition coefficients for the Bow Hill basanite UT-70489 (the experimental starting material for this study), together with previously published partitioning data for halides. For this purpose, partition coefficients were chosen from Table 3 (this study) and Adam and Green (2006), and used to calculate D values for a pyrolite-based upper mantle assemblage (including 10 % garnet +18 % clinopyroxene + 12 % orthopyroxene + 60 % olivine). The data were selected so as to represent as closely as possible conditions of liquidus saturation with garnet lherzolite (~2.7 GPa and 1200 °C) [runs 1955 and 1956 (garnet) at 3.5 GPa and 1180-1190 °C; R80 and 1948 (clinopyroxene and orthopyroxene) at 3.0-2.5 GPa and 1170-1160 °C; and R77 (olivine) at 2.0 GPa and 1100 °C]. The results give $D^{pyrolite/melt}$ for H_2O, La and Ce equal to 0.0052, 0.0052 and 0.0103 respectively. Because H_2O concentrations in our experimentally-produced melts (range 6.8-16.8 weight %) were significantly more than likely in the original basanite magma (~ 4.5 weight %, see Adam 1990) the quoted D value for H_2O is probably an underestimate (see previous discussion of the effects of melt H_2O concentration on D_{H2O}). Thus $D_{H2O}^{pyrolite/melt}$ may resemble $D_{Ce}^{pyrolite/melt}$ more closely than $D_{La}^{pyrolite/melt}$. This is not a major concern because the relative compatibility of H_2O in natural intraplate magmas appears to be variable and may be similar to that of either La or Ce (see Dixon et al. 1988; Michael 1995). Data from Dalou et al. (2012) were used to calculate $D_{Cl}^{pyrolite/melt} \approx 0.0016$, which is very similar to values for Rb and Ba (0.0021 and 0.0016).

If the partitioning data are applied to conditions of origin for the Bow Hill basanite [estimated at ~ 2.7 GPa and 1200 °C with 4.5 weight % of dissolved H_2O and 2.0 weight % of dissolved CO_2 (Adam 1990)] the bulk melting residue will have contained ~ 230 ppm H_2O and 2 ppm Cl [based on 1240 ppm Cl in UT-70489 (from Adam and Green 2011)]. These values are comparable to some previous estimates of H_2O and Cl concentrations in the MORB source (e.g. Saal et al.

2002; Workman and Hart 2005; Green et al. 2010). But the need for a finite degree of melting means that the Bow Hill source is likely to have been significantly more enriched in H_2O, CO_2 and Cl than the MORB source.

Similar conclusions were reached by Adam and Green (2011) with respect to concentrations of incompatible non-volatile elements. They noted that although the relative concentrations of incompatible elements in UT-70489 are consistent with an E-type MORB source (which UT-70489 isotopically resembles), the absolute concentrations are too high to be a direct result of partially melting such a (non-enriched) source. As an alternative, it was suggested that the Bow Hill source was pre-enriched in incompatible elements by metasomatic melts derived from underlying MORB sources. This was modelled by the addition of 30 % of a small degree (0.7 %) partial-melt of the E-MORB source of Workman and Hart (2005) to a depleted peridotite (see Adam and Green 2011). The resulting pyrolite-like composition could have produced UT-70489 by ~ 5.5 % partial-melting. If this same model is used for volatile concentrations, the Bow Hill source would have contained ~ 0.25 weight % H_2O, 0.11 weight % CO_2 and 52 ppm Cl. In spite of such high absolute concentrations, key ratios of volatile and non-volatile elements remain comparable to those in MORB. These include: $H_2O/Ce = 230$, $CO_2/Nb = 140$ and $Cl/K = 0.07$ (by weight). Equivalent values for MORB are: $H_2O/Ce = 200(50)$ (Michael 1995), $CO_2/Nb = 239(36)$ (Saal et al. 2002), and $Cl/K = 0.01$-0.08 (Michael and Cornell 1998).

Alternative models of origin for OIB sources have also been proposed in which the role of volatiles is essentially incidental once they have been subducted into the deeper mantle. These emphasize the coupled significance of subduction zone processes and deep mantle plumes (e.g. Hofmann and White 1982; Dupuy et al. 1989; Hirschmann et al. 2003; Sobolev et al. 2005). A problem with this option (at least in its simplest form) is that H_2O is fractioned differently by

553 subduction zone processes than it is by peridotite melting. This is demonstrated in Fig. 11 which
554 shows relative enrichments of volatile and non-volatile elements in arc magmas and the
555 continental crust/hydrosphere normalized to concentrations in an average MORB. The relative
556 enrichments of H_2O, Pb and other incompatibles mirror experimentally-obtained partitioning
557 relationships for H_2O-fluids (see also Brenan et al. 1995; Keppler 1996; Kessel et al. 2005)
558 and are very different from those in OIB which, with the minor exception of Pb (possibly held in
559 sulphides), mirror peridotite/melt partition coefficients for basanite melts. These relationships do
560 not either preclude or ignore evidence for contributions from re-cycled crustal components to
561 OIB sources, but imply instead that the metasomatic processes responsible for OIB magmatism
562 can superimpose themselves on a wide range of mantle materials (since, as pointed out by
563 Michael (1995), all of the H_2O in the MORB mantle has probably been re-cycled). If this is
564 indeed the case, and both OIB and MORB owe their source characteristics to a common
565 fractionation mechanism, it is likely that this fractionation occurred under specific conditions of
566 pressure, temperature and H_2O activity.

567

568 **SUMMARY AND CONCLUSIONS**

569 Concentrations of H_2O, F, Cl, C and S have been analysed by SIMS in experimentally-produced
570 amphibole, mica, garnet, clinopyroxene, orthopyroxene, olivine and basanitic glass (melts).
571 Concentrations of H_2O in melts were also independently estimated from mass-balance
572 relationships and by assuming constant H_2O/La in melts and starting materials. The data were
573 used to calculate mineral/melt partition coefficients for H_2O (for conditions of 1.0-3.5 GPa and
574 1025-1190 °C), but only limited information could be obtained for the other volatiles. Consistent

575 with observations from previous experimental studies, both $D_{H2O}^{cpx/melt}$ and $D_{H2O}^{opx/melt}$ correlate
576 positively with ^{iv}Al in pyroxenes. But $D_{H2O}^{cpx/melt}$ and $D_{H2O}^{opx/melt}$ are also negatively correlated
577 with H_2O concentrations in melts. Although the same relationship is not demonstrated by the
578 more limited data available for olivine and garnet, it is consistent with key aspects of published
579 solution models for H_2O in silicate melts. D_{H2O}/D_{Ce} for clinopyroxenes and melts is a negative
580 function of the M2 site radius, and can be related to the controlling influence of the M2 site on
581 $D_{Ce}^{cpx/melt}$. Because M2 site radii are themselves a function of pressure and temperature, and
582 pyroxenes exert a controlling influence on the partitioning of both H_2O and Ce, deeply derived
583 melts from relatively hot mantle sources should have lower H_2O/Ce than melts from shallower
584 and cooler (but otherwise equivalent) sources. Because melt-H_2O concentrations also influence
585 the relative partitioning of H_2O and Ce, (H_2O-rich) subduction-zone environments should
586 fractionate H_2O and Ce differently from other mantle settings.

587 The experimentally-determined compatibilities of H_2O, C, F, Cl, Ba, Nb, La, Ce, and Sr are
588 consistent with observed correlations between some volatile and non-volatile components (e.g.
589 H_2O/Ce) in undegassed MORB and OIB glasses. They are also consistent with Michael's (1995)
590 suggestion that intraplate basalt sources are enriched in volatiles and other incompatibles by
591 small-degree melts derived from local MORB sources. In this way, H_2O and other volatiles can
592 be held to play an active role (via their promotion of partial-melting and metasomatic processes)
593 in the auto-regulation of incompatible element concentrations in the depleted upper mantle.

594

Acknowledgements

This study was supported by an ARC Professorial Fellowship to Simon Turner and a New Zealand Foundation of Research in Science and Technology postdoctoral fellowship to Michael Turner. It also made use of instrumentation funded by ARC, LIEF and DEST Systematic Infrastructure Grants, Macquarie University and Industry. Hugh O'Neil is thanked for his comments on an earlier draught of this manuscript. Roland Stalder and István Kovács are also thanked for constructive and thoughtful reviews. This is contribution number 669 from the ARC Centre of Excellence for Core to Crust Fluid Systems (http://www.ccfs.mq.edu.au) and number 1034 from the GEMOC Key Centre for the Geochemical Evolution and Metallogeny of Continents (http://www.gemoc.mq.edu.au).

606 **FIGURE CAPTIONS**

607

608 **Figure 1**

609 Longitudinal sections of experimental capsules showing run products after experiments. Run
610 R79 (Fig. 1a) conducted at 1075 °C and 1.0 GPa produced a red-brown glass containing crystals
611 of olivine and less common clinopyroxene. In Run R80 (Fig. 1b) the melt phase (produced at
612 1170°C and 3.0 GPa) quenched to a felt-like matrix of fine crystallites. Accumulated at the base
613 of the capsule are crystals of clino- and orthopyroxene. Both pictures were taken in ordinary light
614 with a binocular microscope.

615

616 **Figure 2**

617 A comparison of results for the different methods used to estimation H_2O concentrations in the
618 experimentally-produced melts of this study. The diagonal straight line shows a 1:1 relationship.

619

620 **Figure 3**

621 Variation of clinopyroxene/melt D values for H_2O as a function of ^{iv}Al (3a) and melt H_2O
622 concentrations (3b). Also shown is the cross-correlation between ^{iv}Al and the H_2O concentrations
623 of melts (3c). Data for the Bow Hill basanite are from this study and Adam and Green (2006).
624 Other data sources include: Adam and Green (1994), Dobson et al. (1995), Green et al. (2000),
625 Hauri et al. (2006), Koga et al. (2003), Aubaud et al. (2004, 2008), Tenner et al. (2009), O'Leary

et al. (2010) and Kovacs et al. (2012). D values were estimated from the data of Kovacs et al. (2012) by assuming melt-H_2O solubilities of ~ 10 weight % per GPa (see text). Except for the basanite from Bow Hill (UT-70489, the subject of this work), symbols and author's names correspond to the original experimental studies used to produce crystals and melts.

Figure 4

Variations in F concentrations and ^{iv}Al in the experimentally produced pyroxenes of this study.

Figure 5

Variation of orthopyroxene/melt D values for H_2O as a function of ^{iv}Al (5a) and melt H_2O concentrations (5b). Data for the Bow Hill basanite are from this study and Adam and Green (2006). Other data sources include: Dobson et al. (1995), Gaetani and Grove (1998), Green et al. (2000), Aubaud et al. (2004), Koga et al. (2003), Hauri et al. (2006), Tenner et al. (2009) and Kovács et al. (2012). D values were estimated from the data of Kovács et al. (2012) by assuming melt-H_2O solubilities of ~ 10 weight % per GPa (see text). Except for the basanite from Bow Hill (UT-70489, the subject of this work), symbols and author's names correspond to the original experimental studies used to produce crystals and melts.

Figure 6

Variation of olivine/melt D values for H_2O as a function of melt H_2O concentrations (5a) and pressure (b). Data for the Bow Hill basanite are from this study. Other data sources include:

Koga et al. (2003), Aubaud et al. (2004), Hauri et al. (2006), Grant et al. (2007), Kovács et al. (2012), Tenner et al. (2012) and Novella et al. (2014). D values were estimated from the Kovács et al. (2012) data by assuming melt-H_2O solubilities of ~ 10 weight % per GPa (see text). Except for the basanite from Bow Hill (UT-70489, the subject of this work), symbols and author's names correspond to the original experimental studies used to produce crystals and melts.

Figure 7

Variation of garnet/melt D values for H_2O as a function of melt H_2O concentrations. Data sources include: this study, Hauri et al. (2006), Aubaud et al. (2008), Tenner et al. (2009) and Novella et al. (2014). Except for the basanite from Bow Hill (UT-70489, the subject of this work), symbols and author's names correspond to the original experimental studies used to produce crystals and melts.

Figure 8

Mole fractions of OH^- versus weight % H_2O in basanite melts (a) calculated using Burnham's (1975) albite-based model for the solution of H_2O in silicate melts; and (b) accompanying variations in $D_{H2O}^{cpx/melt}$ calculated for a constant exchange $K_D = 0.0014$ (see text). Sources for other accompanying data are as for Fig. 3b.

Figure 9

(a) Calculated mole fractions of OH^- and molecular H_2O versus weight % of total H_2O in silicate melts at 1150 °C (based on Sowerby and Keppler (1999) where ln k = -3821.83/T + 1.61); and (b) resultant variations in $D_{H2O}^{cpx/melt}$ (solid line) calculated assuming $D_{OH}^{cpx/melt}$ = 0.05 and that H_2O dissolves in pyroxenes only as OH^-. Sources for other plotted data are as for Fig. 3b.

Figure 10

Variations in D_{H2O}/D_{Ce} for clinopyroxene as a function of: (a) average M2-O distance, (b) X_{Ca}, and (c) r_0^{+3} values for M2 sites. Error bars show propagated single standard deviations. The M2-O distances are unpublished data of Adam, Oberti and Camara [for methods see Adam et al. (2007)]. Data for D_{H2O}, D_{Ce}, Ca and r_0^{+3} values are from Table 2 (this study), Hauri et al. (2006), Adam and Green (2003, 2006) and Green et al. (2000).

Figure 11

Bulk partition coefficients for garnet lherzolite/basanite melt and garnet lherzolite/H_2O-fluid. Also shown are the relative enrichments of volatile and non-volatile incompatible elements in intraplate basalts, the continental crust/hydrosphere, and three different arc magmas. These are shown normalized to an average mid-ocean-ridge basalt composition from Albarede (2005) with H_2O, CO_2 and halides based on data for H_2O/Ce, CO_2/Nb, Cl/K and F/P from Michael (1995) and Saal et al. (2002). The partition coefficients for basanitic melts are mostly based on data from this work and Adam and Green (2006) [see text]. The exceptions are Cl and F which are from Dalou et al. (2012). The partition coefficients for H_2O-fluids are based on this work, Adam

and Green (2006), and Adam et al. (2014). The composition of the combined continental crust and hydrosphere is based on data from Wedepohl (Table 3, 1995), Schubert and Sandwell (1989), and Shiklomanov and Rodda (Table 1.8, 2003). The data for undegassed arc magmas are from Rose et al. (1978), Sisson and Layne (1993), Scaillet and Evans (1999), Borisova et al. (2006), and Johnson et al. (2009).

694

695 **REFERENCES CITED**

696 Adam, J. (1990) The geochemistry and experimental petrology of sodic alkaline basalts from
697 Oatlands, Tasmania. Journal of Petrology, 31, 1201-1223.

698 Adam, J., and Green, T.H. (2003) The influence of pressure, mineral composition and water on
699 trace element partitioning between clinopyroxene, amphibole and basanitic melts. European
700 Journal of Mineralogy, 15, 831-841.

701 Adam, J., and Green, T.H. (2006) Trace element partitioning between mica- and amphibole-
702 bearing garnet lherzolite and hydrous basanitic melt: 1. Experimental results and the
703 investigation of controls on partitioning behaviour. Contributions to Mineralogy and Petrology,
704 152, 1-17. DOI 10.1007/s00410-006-0085-4.

705 Adam, J., Oberti, R., Camara, F., and Green, T.H. (2007) An electron microprobe, LAM-ICP-
706 MS and single-crystal X-ray structure refinement study of the effects of pressure, melt-H_2O
707 concentration and fO_2 on experimentally produced basaltic amphiboles. European Journal of
708 Mineralogy, 19, 641-655. DOI 10.1127/0935-1221/2007/0019-1750.

709 Adam, J., and Green, T.H. (2011) Trace element partitioning between mica- and amphibole-
710 bearing garnet lherzolite and hydrous basanitic melt: 2. Tasmanian Cainozoic basalts and the
711 origins of intraplate basaltic magmas. Contributions to Mineralogy and Petrology, 161, 883-899.
712 DOI 10.1007/s00410-010-0570-7.

Adam, J., Locmelis, M., Afonso, J.C., Rushmer, T., and Fiorentini, M. (2014) The capacity of hydrous fluids to transport and fractionate incompatible elements and metals within the Earth's mantle. Geochemistry Geophysics Geosystems, DOI 10.1002/2013GC005199.

Aines, R.D., and Rossman, G.R. (1984) Water content of mantle garnets. Geology 12: 720-723

Albarede, F. (2005) The survival of geochemical heterogeneities. In: Earth's Deep Mantle: Structure, Composition and Evolution. Geophysical Monograph van der Hilst R.D., Bass J., Matas J., and Trampert, J. (eds) Washington D. C., American Geophysical Union, 160, pp. 27-46.

Aubaud, C., Hauri, E.H., and Hirschmann, M.M. (2004) Hydrogen partition coefficients between nominally anhydrous minerals and basaltic melts. Geophysical Research Letters, 31, L20611 doi: 10.1029/2004GL021341.

Aubaud, C., Hirschmann, M.M., Withers, A.C., and Hervig, R.L. (2008) Hydrogen partitioning between melt, clinopyroxene, and garnet at 3 GPa in a hydrous MORB with 6 wt. % H_2O. Contributions to Mineralogy and Petrology, 156, 607-625.

Bell, D.R., and Rossman, G.R. (1992) Water in Earth's Mantle: The role of nominally anhydrous minerals. Science, 255, 1391-1331.

Behrens, H., Misiti, V., Freda, C., Vetere, F., Botcharnikov, R.E., and Scarlato, P. (2009) Solubility of H_2O and CO_2 in ultrapotassic melts at 1200 and 1250 °C and pressure from 50 to 500 MPa. American Mineralogist, 94, 105-120.

Beyer, C., Klemme, S., Wiedenbeck, M., Stracke, A., and Vollmer, C. (2012) Flourine in nominally fluorine-free mantle minerals: experimental partitioning of F between olivine,

orthopyroxene and silicate melts with implications for mantle processes. Earth and Planetary Science Letters, 337, 1-9.

Blundy, J., and Wood, B.J. (1994) Prediction of crystal-melt partition coefficients from elastic moduli. Nature, 372, 452-454.

Borisova, A.Y., Pichavant, M., Polvé, M., Wiedenbeck, M., Freydier, R., and Candaudap, F. (2006) Trace element geochemistry of the 1991 Mt. Pinatubo silicic melts, Philippines: Implications for ore-forming potential of adakitic magmatism. Geochimica et Cosmochimica Acta, 70, 3702-3716.

Brenan, J.M., Shaw, H.F., Ryerson, F.J., and Phinney, D.L. (1995) Mineral-aqueous fluid partitioning of trace elements at 900 C and 2.0 GPa: constraints on the trace element chemistry of mantle and deep crustal fluids. Geochimica et Cosmochimica Acta, 59, 3331-3350.

Brey, G. and Green, D.H. (1977) Systematic study of liquidus phase relations in olivine melilitite + H_2O + CO_2 at high pressures and petrogenesis of an olivine melilitite magma. Contributions to Mineralogy and Petrology, 61, 141-162.

Burnham, C.W. (1975) Water and magmas: a mixing model. Geochimica et Cosmochimica Acta, 39, 1077-1084.

Carroll, M.R., and Blank, J.G. (1997) The solubility of H_2O in phonolite melts. American Mineralogist, 82, 549-556.

753 Dalou, C., Koga, K.T., Shimizu, N., Boulon, J., and Devidal, J. (2012) Experimental
754 determination of F and Cl partitioning between lherzolite and basaltic melt. Contributions to
755 Mineralogy and Petrology, 163, 591-609. DOI: 10.1007/s00410-011-0688-2.

756 Dixon, J.E., Stolper, E., and Delaney, J.R. (1988) Infrared spectroscopic measurements of CO_2
757 and H_2O in Jaun de Fuca Ridge basaltic glasses. Earth and Planetary Science Letters, 90, 87-104.

758 Dobson, P., Skogby, H., and Rossman, G.R. (1995) Water in boninite glass and coexisting
759 orthopyroxene: concentration and partitioning. Contributions to Mineralogy and Petrology, 118,
760 414-419.

761 Dupuy, C., Barsczus, H., Dostal, J., Vidal, P., and Liotard, J. (1989) Subducted and recycled
762 lithosphere as the mantle source of ocean island basalts from southern Polynesia, Central Pacific.
763 Earth and Planetary Science Letters, 114, 477-489.

764 Eggler, D.H., and Burnham, C.W. (1984) Solution of H_2O in diopside melts: a thermodynamic
765 model. Contributions to Mineralogy and Petrology, 85, 58-66.

766 Gaetani, G.A., and Grove, T.L. (1998) The influence of water on melting of mantle peridotite.
767 Contributions to Mineralogy and Petrology, 131, 323-346.

768 Grant, K.J., Kohn, S.C., and Brooker, R.A. (2007) The partitioning of water between olivine,
769 orthopyroxene and melt synthesised in the system albite-forsterite-H_2O. Earth and Planetary
770 Science Letters, 260, 227-241.

771 Green, D.H. (1976) Experimental testing of "equilibrium" partial melting of peridotite under
772 water-saturated, high-pressure conditions. Canadian Mineralogist, 14, 255-268.

773 Green, D.H., Hibberson , W.O., Kovács, I., and Rosenthal, A. (2010) Water and its influence on
774 the lithosphere-asthenosphere boundary. Nature, 467, 448-452. DOI: 10.1038/nature09369

775 Green, T.H., Blundy, J.D., Adam, J., and Yaxley, G.M. (2000) SIMS determination of trace
776 elements partition coefficients between garnet, clinopyroxene and hydrous basaltic liquids at 2-
777 7.5 GPa and 1080-1200 °C. Lithos, 53, 165-187.

778 Hauri, E.H., Wang, J., Dixon, J.E., King, P.L., Mandeville, C., and Newman, S. (2002) SIMS
779 analysis of volatiles in silicate glasses 1. Calibration, matrix effects and comparisons with FTIR.
780 Chemical Geology, 183, 99-114.

781 Hauri, E.H., Gaetani, G.A., and Green, T.H. (2006) Partitioning of water during melting of the
782 Earth's upper mantle at H_2O undersaturated conditions: Earth and Planetary Science Letters, 248,
783 715-734. DOI: 10.1016/j.epsl.2006.06.014.

784 Hervig, R.L., and Bell, D.R. (2005) Fluorine and hydrogen in mantle megacrysts. AGU Fall
785 Meeting, pp. V41A-1426.

786 Hirschmann, M.M., and Dasgupta, R. (2009) The H/C ratios of Earth's near-surface and deep
787 reservoirs, and consequences for deep Earth volatile cycles. Chemical Geology, 262, 2-16.

788 Hirschmann, M.M., Kogiso, T., Baker, M.B., and Stolper, E.M. (2003) Alkalic magmas
789 generated by partial melting of garnet pyroxenite. Geology, 31, 481-484.

790 Hofmann, A.W., and White, W.M. (1982) Mantle plumes from ancient oceanic crust. Earth and
791 Planetary Science Letters, 57, 421-436.

Holloway, J.R., Pan, V., and Gudmundsson, G. (1992) High-pressure fluid-absent melting experiments in the presence of graphite : oxygen fugacity, ferric/ferrous ratio and dissolved CO_2. European Journal of Mineralogy, 4, 105-114. DOI: 0935-1221/92/0004-0105.

Jakobsson, S. (1997) Solubility of water and carbon dioxide in an icelandite at 1400 °C and 10 kilobars. Contributions to Mineralogy and Petrology, 127, 129-135.

Jambon, A. (1994) Earth degassing and large scale geochemical cycling of volatile elements. In: Carroll, M.R. and Holloway, J.R. (eds) Volatiles in Magmas, Reviews in Mineralogy, 30, 478-517. Mineralogical Society of America, Washington, D.C.

Johnson, E.R., Wallace, P.J., Grandos, H.D., Manea, V.C., Kent, A.J.R., Bindeman, I.N., and Johnson, R.W. (1989) Intraplate Volcanism in eastern Australia and New Zealand. Cambridge University Press, Cambridge

Johnson, E.R., Wallace, P.J., Delgado Granados, H., Manea, V.C., Kent, A.J.R., Bindeman, I.N., and Donegan, C.S. (2009) Subduction-related volatile recycling and magma generation beneath Central mexico: insights from melt inclusions, oxygen isotopes and geodynamic models. Journal of Petrology, 50, 1729-1764.

Keppler, H. (1996) Constraints from partitioning experiments on the composition of subduction zone fluids. Nature, 380, 237-240.

Kessel, R., Schmidt, M.W., Ulmer, P., and Pettke, T. (2005) Trace element signature of subduction-zone fluids, melts and supercritical liquids at 120-180 km depth. Nature, 437, 725-727.

Koga, K., Hauri, E.H., Hirschmann, M.M., and Bell, D.R. (2003) Hydrogen concentration analyses using SIMS and FTIR: Comparison and calibration for nominally anhydrous minerals. Geochemistry, Geophysics, Geosystems, 4, DOI 10.1029/2002GC000378.

Kohn, S.C. (1996) Solubility of H_2O in nominally anhydrous mantle minerals using ^1H MAS NMR. American Mineralogist, 81, 1523-1526.

Kovács, I., Green, D.H., Rosenthal, A., Hermann, J., O'Neill, H., Hibberson, W.O., and Udvardi, B. (2012) An experimental study of water in nominally anhydrous minerals in the upper mantle near the water-saturated solidus. Journal of Petrology, 53, 2067-2093 DOI 10.1093/petrology/egs044.

Michael, P.J. (1995) Regionally distinctive sources of depleted MORB: evidence from trace elements and H_2O. Earth and Planetary Science Letters, 131, 301-320.

Michael, P.J., and Cornall, W.C. (1998) Influence of spreading rate and magma supply on crystallization and assimilation beneath mid-ocean ridges: evidence from chlorine and major element chemistry of mid-ocean ridge basalts. Journal of Geophysical Research, 103, 18325-18356. DOI 10.1002/jgrb.v103.B8/issuetoc.

Michael, P., and Graham, D. (2013) Concentration and behaviour of CO_2 in MORB and OIB: A reevaluation. Abstract, Goldschmidt Conference, DOI: 10.1180/minmag.2013.077.5.1

Morgan, W.J. (1971) Convection plumes in the lower mantle. Nature, 230, 42-43.

Novella, D., Frost, D.J., Hauri, E.H., Bureau, H., Raepsaet, C., and Roberge, M. (2014) The distribution of H_2O between silicate melt and nominally anhydrous peridotite and the onset of hydrous melting in the deep upper mantle. Earth and Planetary Science Letters, 400, 1-13.

Nowak, M., and Behrens, H. (1995) The speciation of water in haplogranitic glasses and melts determined by in situ near-infrared spectroscopy. Geochimica et Cosmoschimica Acta, 59, 3445-3450.

836 Oberti, R., Ungaretti, L., Cannillo, E., and Hawthorne, F.C. (1993) The mechanism of Cl
837 incorporation in amphibole. American Mineralogist, 7, 1049-1063.

838 O'Leary, J.A., Gaetani, G.A., and Hauri, E.H. (2010) The effect of tetrahedral Al^{3+} on the
839 partitioning of water between clinopyroxene and silicate melt. Earth and Planetary Science
840 Letters, 297, 111-120. DOI: 10.1016/j.epsl.2010.06.011.

841 Pilet, S., Hernandez, J., Sylvester, P., and Poujol, M. (2005) The metasomatic alternative for
842 ocean island basalt chemical heterogeneity. Earth and Planetary Science Letters, 236, 148-166.

843 Pouchou, J.L., and Pichoir, F. (1984) A new model for quantitative X-ray microanalysis, Part I.
844 application to the analysis of homogeneous samples. La Recherche Aérospatiale, 3, 13-38.

845 Putirka, K.D., Pelt, M., Ryerson, F.J., and Jackson, M.G. (2007) Ambient and excess mantle
846 temperatures , olivine thermometry, and active vs. passive upwelling. Chemical Geology, 241,
847 177-206.

848 Rose, W.I., Anderson, A.T., Woodruf, L.G., and Bonis, S.B. (1978) The October 1974 basaltic
849 tephra from Fuego Volcano: description and history of the magma body. Journal of Volcanology
850 and Geothermal Research, 4, 3-53.

851 Saal, A.E., Hauri, E.H., Langmuir, C.H., and Perfit, M.R. (2002) Vapour undersaturation in
852 primitive mid-ocean-ridge basalt and the volatile content of the Earth's upper mantle. Nature,
853 419, 451-455.

854 Scaillet, B., and Evans, B.W. (1999) The 15 June 1991 Eruption of Mount Pinatubo. I. Phase
855 equilibria and pre-eruption P-T-fO_2-fH_2O conditions of the dacite magma. Journal of Petrology,
856 40, 381-412.

Schilling, J-G., Bergeron, M.B., and Evans, R. (1980) Halogens in the mantle beneath the North Atlantic. Philosophical Transactions of the Royal Society of London, A297, 147-178.

Schmidt, B.C., and Behrens, H. (2008) Water solubility in phonolite melts: Influence of melt composition and temperature. Chemical Geology, 256, 259-268.

Schubert, G., and Sandwell, D. (1989) Crustal volumes of the continents and of oceanic and continental submarine plateaus. Earth and Planetary Science Letters, 92, 234-246.

Shannon, R.D. (1976) Revised effective ionic radii and systematic studies of interatomic distances in halides and chalcogenides. Acta Crystallographica, A32, 751-767.

Shcheka, S.S., Wiedenbeck, M., Frost, D.J., and Keppler, H. (2006) Carbon solubility in mantle minerals. Earth and Planetary Science Letters, 245, 730-742.

Shiklomanov, I.A., and Rodda, J.C. (2003) *World water resources at the beginning of the twenty-first Century.* International Hydrology Series, UNESCO, Cambridge University Press, Cambridge, pp. 13.

Silver, L.A., and Stolper, E. (1985) A thermodynamic model for hydrous silicate melts. Journal of Geology, 93, 161-178.

Silver, L.A., Ihinger, P.D., and Stolper, E. (1990) The influence of bulk composition on the speciation of water in silicate glasses. Contributions to Mineralogy and Petrology, 104, 142-162.

Sisson, T.W., and Layne, G.D. (1993) H_2O in basalt and basaltic andesite glass inclusions from four subduction-related volcanoes. Earth and Planetary Science Letters, 117, 619-635.

Sobolev, A.V., Hofmann, A.W., Sobolev, S.V., and Nikogosian, I.K. (2005) An olivine-free mantle source of Hawaiian shield basalts. Nature, 434, 590-597.

Sowerby, J.R., and Keppler, H. (1999) Water speciation in rhyolitic melts determined by in-situ infrared spectroscopy. American Mineralogist, 84, 1843-1849.

Stalder, R. (2004) Influence of Fe, Cr and Al on hydrogen incorporation in orthopyroxene. European Journal of Mineralogy, 16, 703-711.

Sutherland, F.L., Hollis, J.D., and Barron, L.M. (1984) Garnet lherzolite and other inclusions from a basalt flow, Bow Hill, Tasmania. In Kornprobst, J. (ed.) Kimberlites II: The Mantle and Crust-Mantle Relationships pp. 145-160. Elsevier, Amsterdam.

Tenner, T.J., Hirschmann, M.M., Withers, A.C., and Hervig, R.L. (2009) Hydrogen partitioning between nominally anhydrous upper mantle minerals and melt between 3 and 5 GPa and applications to hydrous peridotite partial melting. Chemical Geology, 262, 42-56, DOI: 10.1016/j.chemgeo.2008.12.006.

Tenner, T.J., Hirschmann, M.M., Withers, A.C., and Ardia, P. (2012) H_2O storage capacity of olivine and low-Ca pyroxene from 10 to 13 GPa: Consequences for dehydration melting above the transition zone. Contributions to Mineralogy and Petrology, 163, 297-316, DOI:10.1007/s00410-011-0675-7.

Wedepohl, K.H. (1995) The composition of the continental crust. Geochimica et Cosmochimica Acta, 59, 1217-1232.

Wilkins, R.W. T., and Sabine, W. (1973) Water content of some nominally anhydrous silicates. American Mineralogist, 58, 508-516.

Wooley, A.R. and Kempe, D.R. (1989) Carbonatites: nomenclature, average chemical compositions, and element distribution. In Bell, K (ed) Carbonatites, Genesis and Evolution pp. 1-14. Unwyn Hymen, London

Workman, R.K., and Hart, S.R. (2005) Major and trace element composition of the depleted MORB mantle (DMM). Earth Planet Sci Lett 231: 53-72

Workman, R.K., Hauri, E., Hart, S.R., Wang, J., and Blusztajn, J. (2006) Volatile and trace elements in basaltic glasses from Samoa: Implications for water distribution in the mantle. Earth Planet Sci Lett 241: 932-951

This is a preprint, the final version is subject to change, of the American Mineralogist (MSA)
Cite as Authors (Year) Title. American Mineralogist, in press.
(DOI will not work until issue is live.) DOI: http://dx.doi.org/10.2138/am-2016-5437

Fig. 1

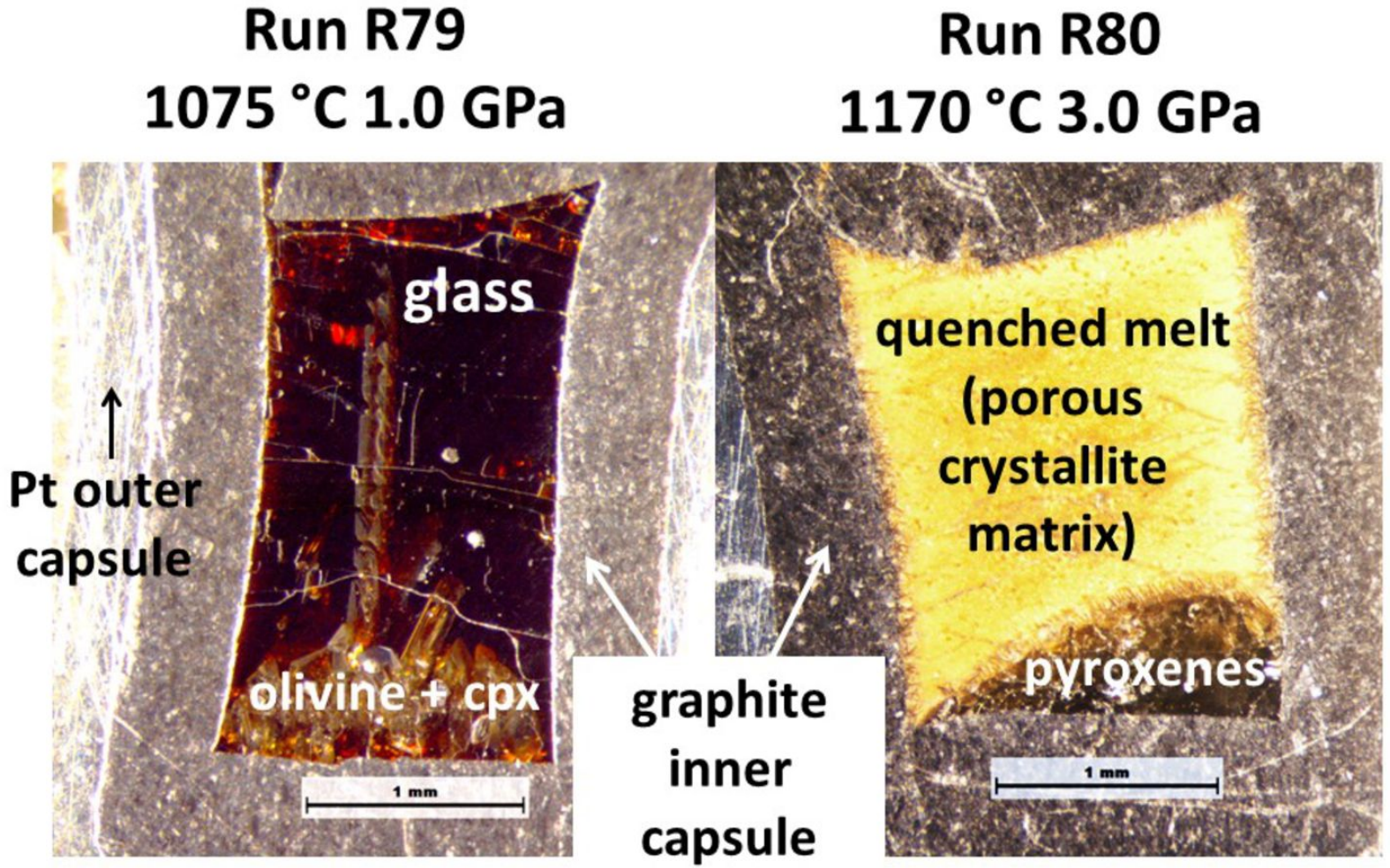

Fig. 2

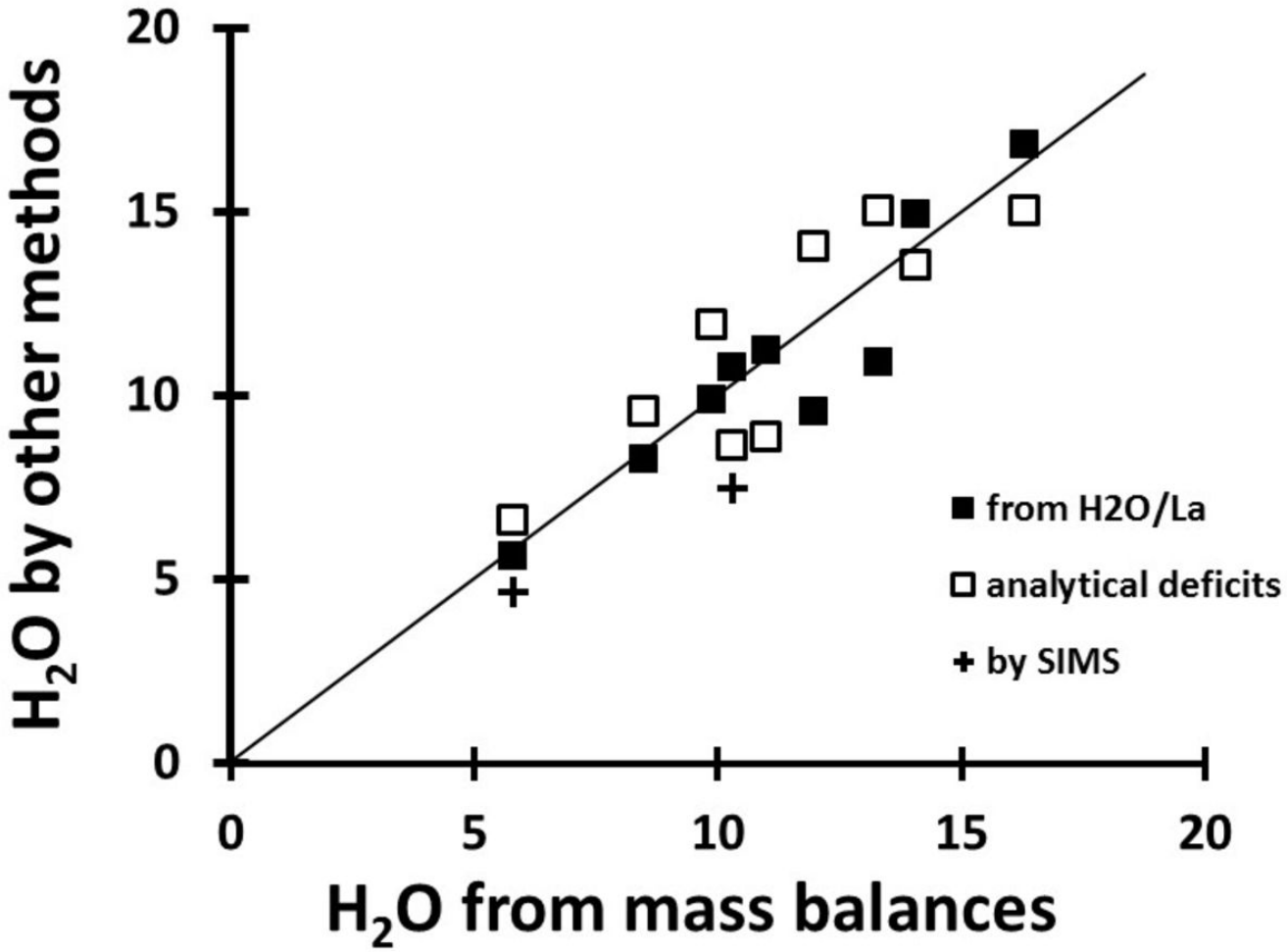
20
15
10
5
0
0
5
10
15
20
H_2O by other methods
H_2O from mass balances
from H2O/La
analytical deficits
by SIMS

This is a preprint, the final version is subject to change, of the American Mineralogist (MSA)
Cite as Authors (Year) Title. American Mineralogist, in press.
(DOI will not work until issue is live.) DOI: http://dx.doi.org/10.2138/am-2016-5437

Fig. 3a

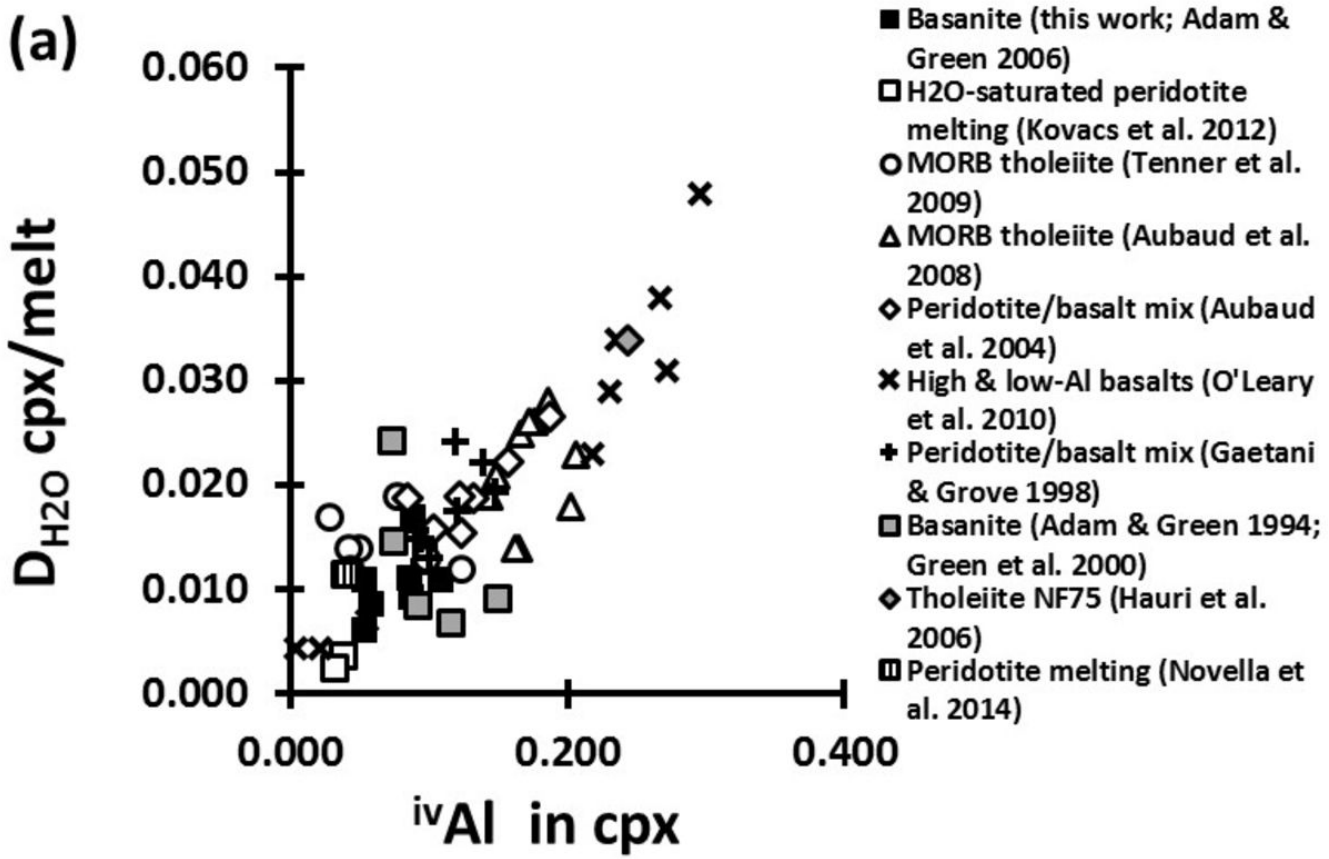

This is a preprint, the final version is subject to change, of the American Mineralogist (MSA)
Cite as Authors (Year) Title. American Mineralogist, in press.
(DOI will not work until issue is live.) DOI: http://dx.doi.org/10.2138/am-2016-5437

Fig. 3b

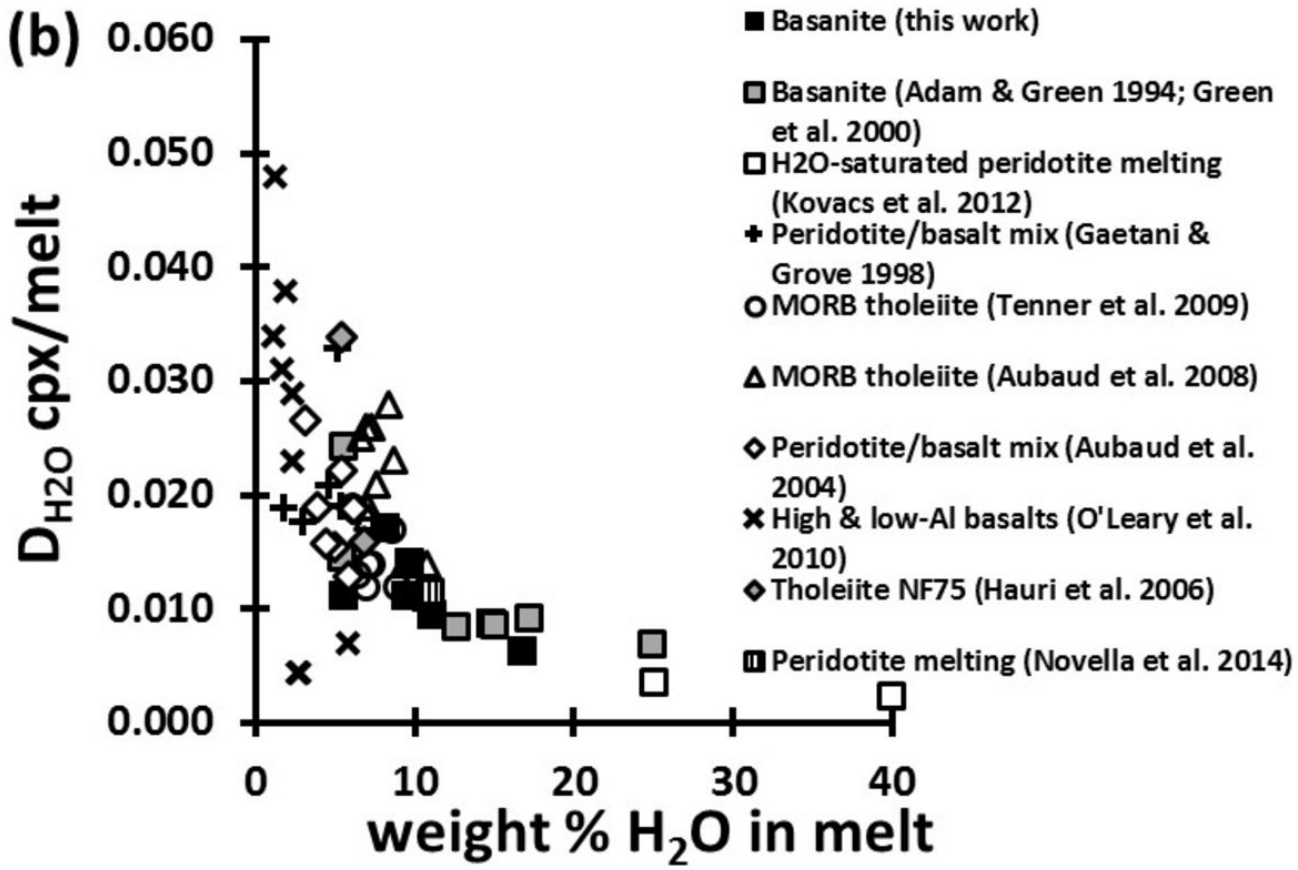

Fig. 3c

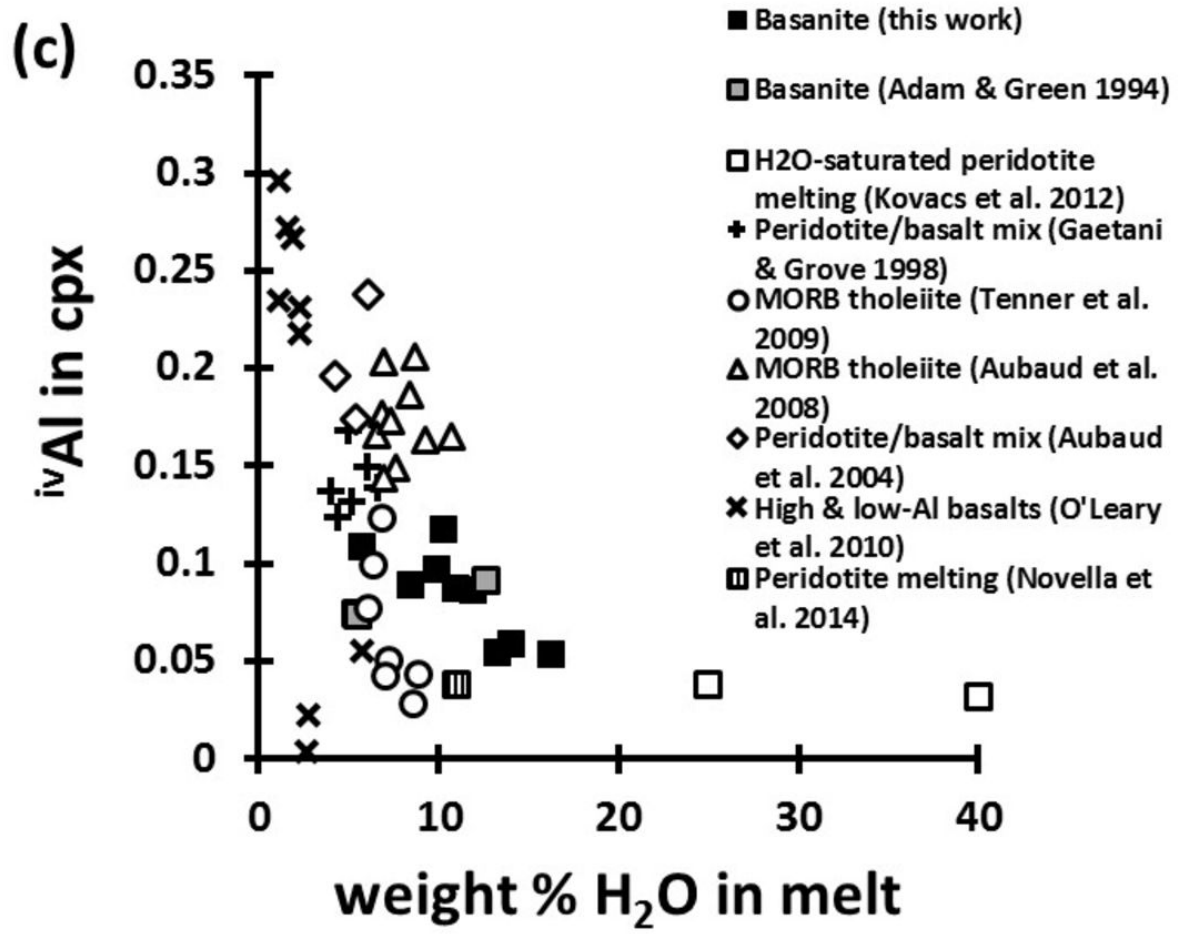
(c)
0.35
0.3
0.25
0.2
0.15
0.1
0.05
0
^{iv}Al in cpx
0
10
20
30
40
weight % H_2O in melt
Basanite (this work)
Basanite (Adam & Green 1994)
H2O-saturated peridotite melting (Kovacs et al. 2012)
Peridotite/basalt mix (Gaetani & Grove 1998)
MORB tholeiite (Tenner et al. 2009)
MORB tholeiite (Aubaud et al. 2008)
Peridotite/basalt mix (Aubaud et al. 2004)
High & low-Al basalts (O'Leary et al. 2010)
Peridotite melting (Novella et al. 2014)

Fig. 4

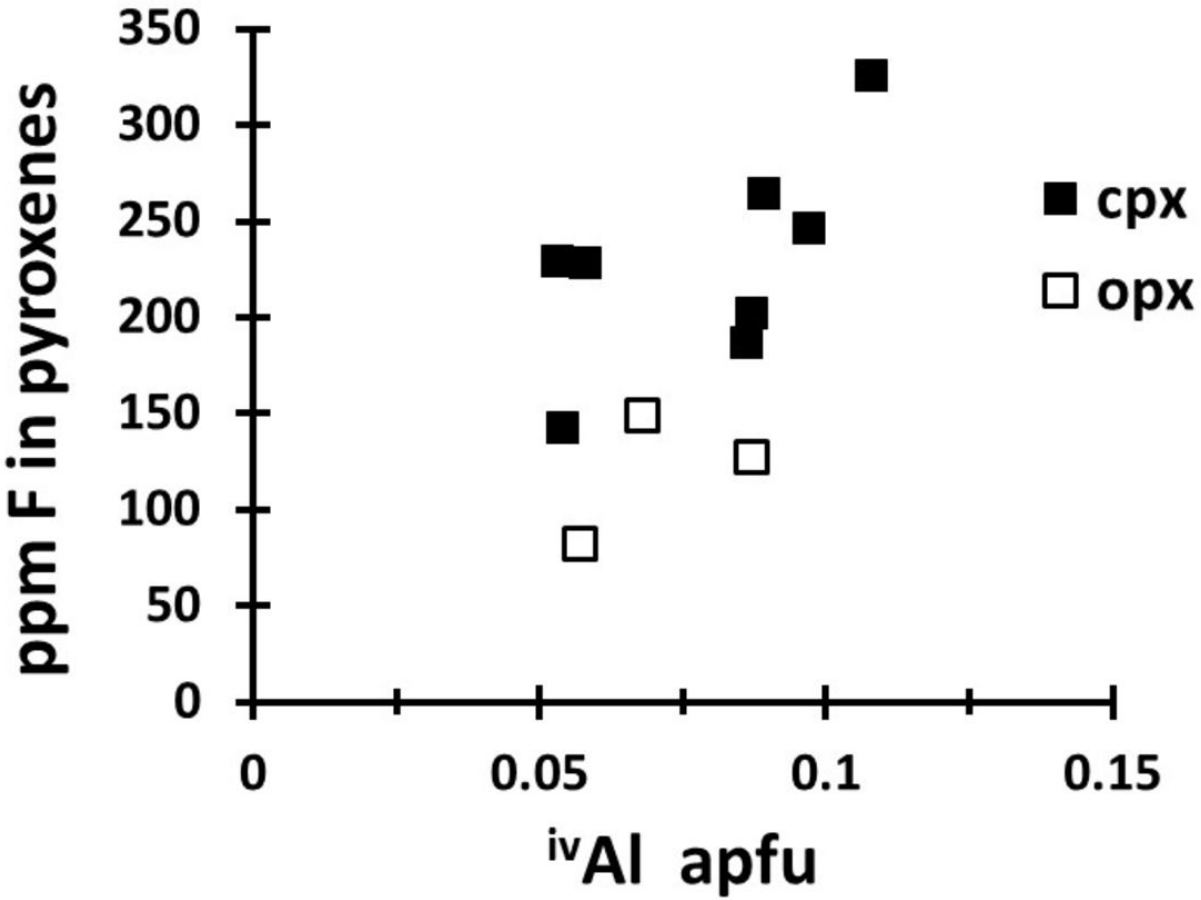
ppm F in pyroxenes
350
300
250
200
150
100
50
0
0
0.05
0.1
0.15
ivAl apfu
cpx
opx

This is a preprint, the final version is subject to change, of the American Mineralogist (MSA)
Cite as Authors (Year) Title. American Mineralogist, in press.
(DOI will not work until issue is live.) DOI: http://dx.doi.org/10.2138/am-2016-5437

Fig. 5a

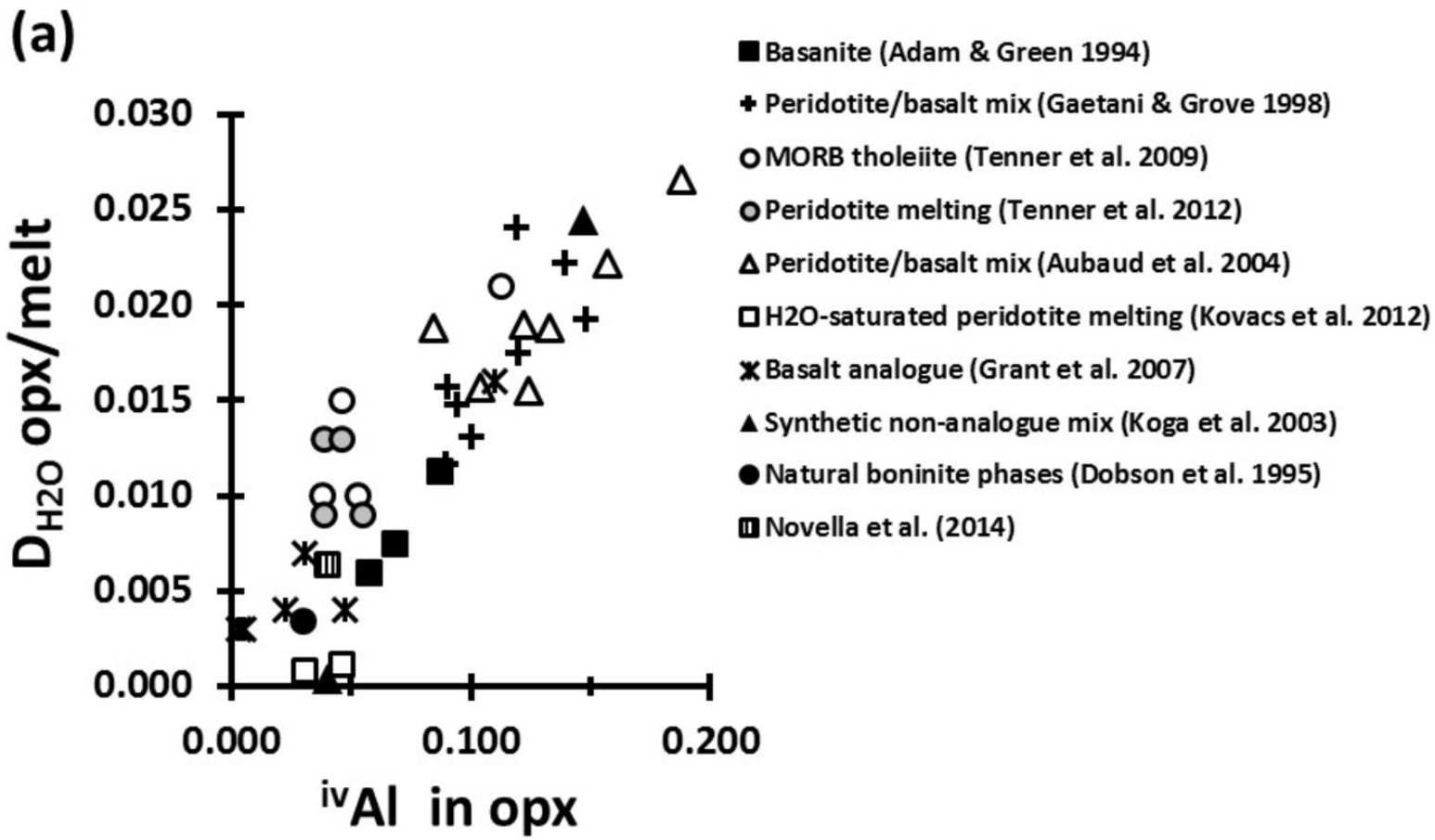

Fig. 5b

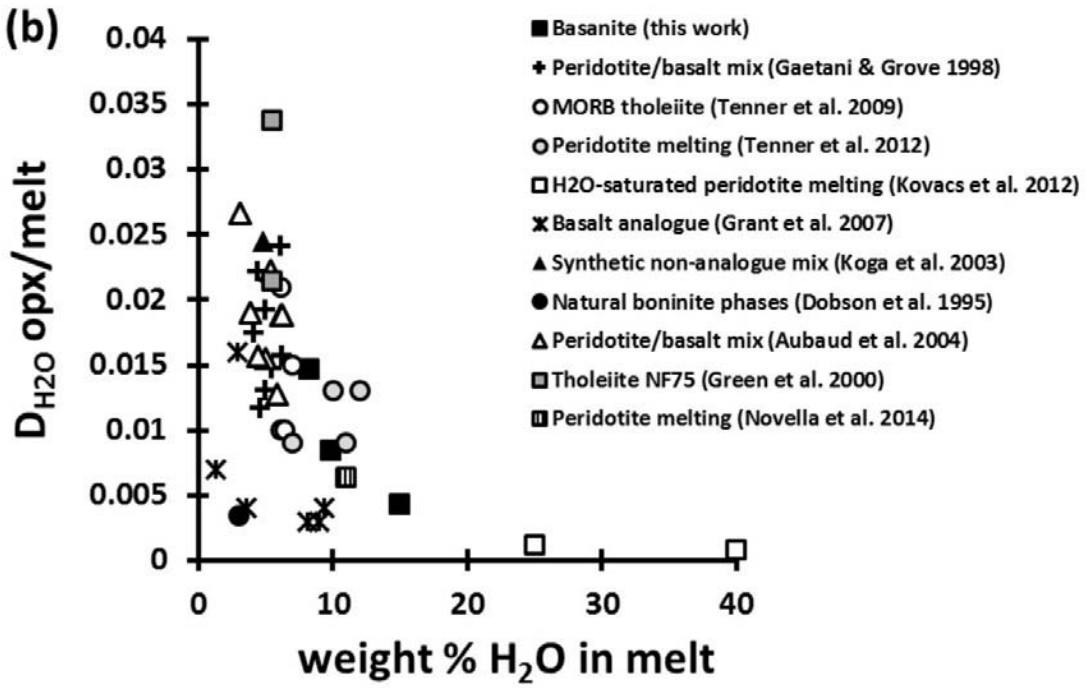
(b)
0.04
0.035
0.03
0.025
0.02
0.015
0.01
0.005
0
D_{H2O} opx/melt
0
10
20
30
40
weight % H_2O in melt
Basanite (this work)
Peridotite/basalt mix (Gaetani & Grove 1998)
MORB tholeiite (Tenner et al. 2009)
Peridotite melting (Tenner et al. 2012)
H2O-saturated peridotite melting (Kovacs et al. 2012)
Basalt analogue (Grant et al. 2007)
Synthetic non-analogue mix (Koga et al. 2003)
Natural boninite phases (Dobson et al. 1995)
Peridotite/basalt mix (Aubaud et al. 2004)
Tholeiite NF75 (Green et al. 2000)
Peridotite melting (Novella et al. 2014)

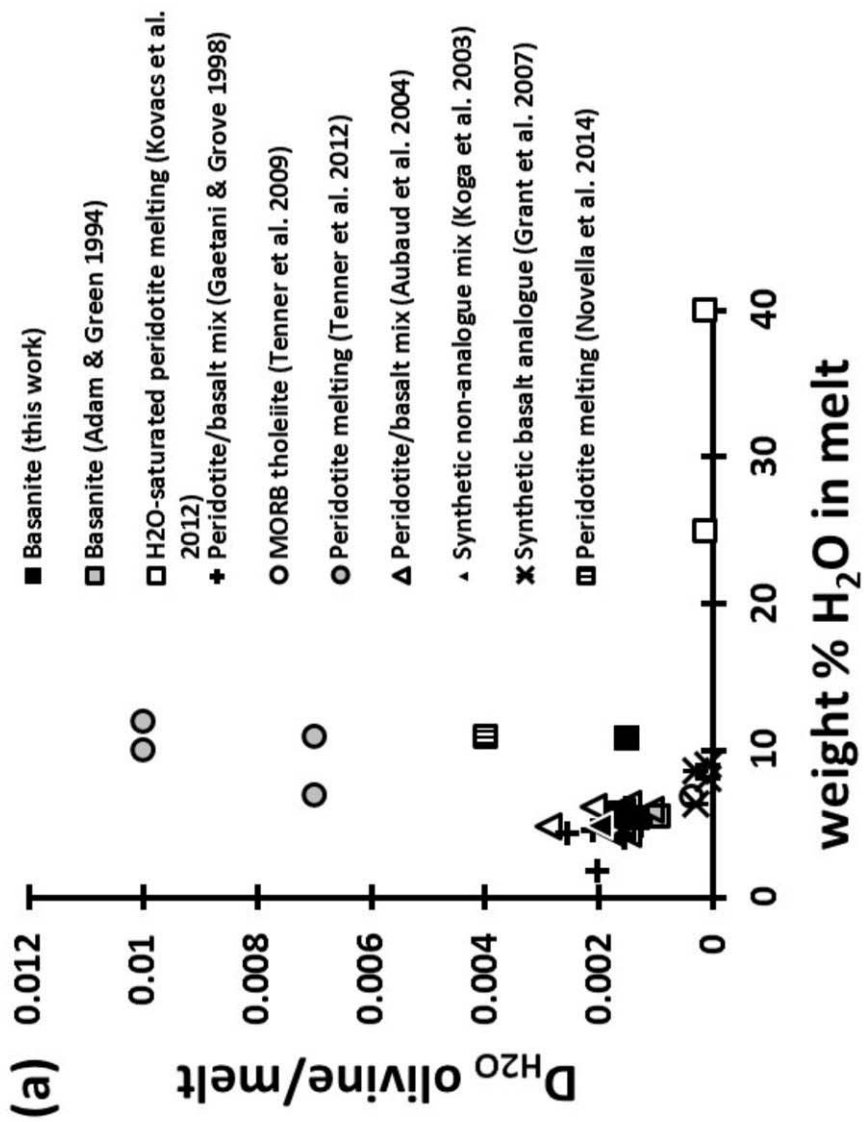
(a)
D_{H2O} olivine/melt
0.012
0.01
0.008
0.006
0.004
0.002
0
0
10
20
30
40
weight % H_2O in melt
Basanite (this work)
Basanite (Adam & Green 1994)
H2O-saturated peridotite melting (Kovacs et al. 2012)
Peridotite/basalt mix (Gaetani & Grove 1998)
MORB tholeiite (Tenner et al. 2009)
Peridotite melting (Tenner et al. 2012)
Peridotite/basalt mix (Aubaud et al. 2004)
Synthetic non-analogue mix (Koga et al. 2003)
Synthetic basalt analogue (Grant et al. 2007)
Peridotite melting (Novella et al. 2014)

Fig. 6a

Fig. 6b

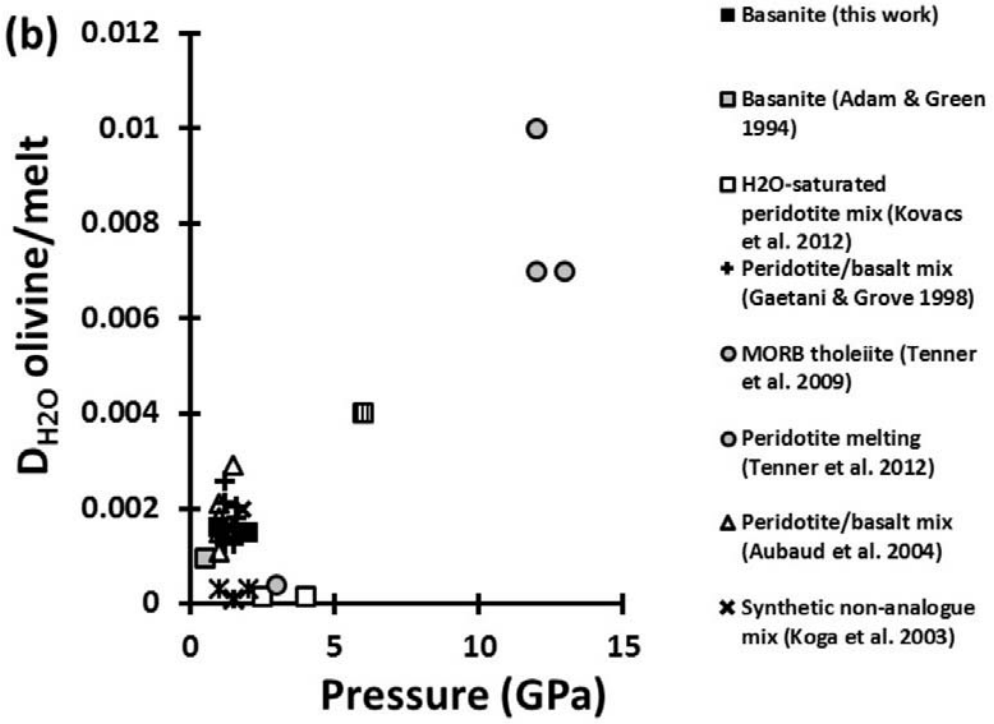
(b)
0.012
0.01
0.008
0.006
0.004
0.002
0
D_{H2O} olivine/melt
0
5
10
15
Pressure (GPa)
Basanite (this work)
Basanite (Adam & Green 1994)
H2O-saturated peridotite mix (Kovacs et al. 2012)
Peridotite/basalt mix (Gaetani & Grove 1998)
MORB tholeiite (Tenner et al. 2009)
Peridotite melting (Tenner et al. 2012)
Peridotite/basalt mix (Aubaud et al. 2004)
Synthetic non-analogue mix (Koga et al. 2003)

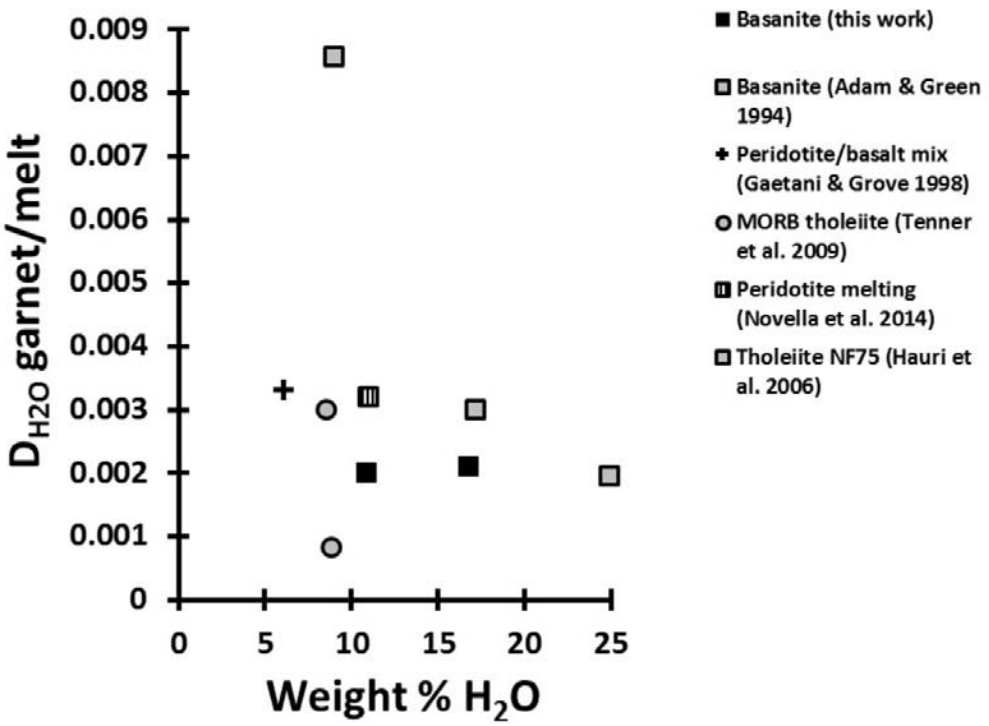
0.009
0.008
0.007
0.006
0.005
0.004
0.003
0.002
0.001
0
D_{H2O} garnet/melt
0
5
10
15
20
25
Weight % H_2O
Basanite (this work)
Basanite (Adam & Green 1994)
Peridotite/basalt mix (Gaetani & Grove 1998)
MORB tholeiite (Tenner et al. 2009)
Peridotite melting (Novella et al. 2014)
Tholeiite NF75 (Hauri et al. 2006)

Fig. 8

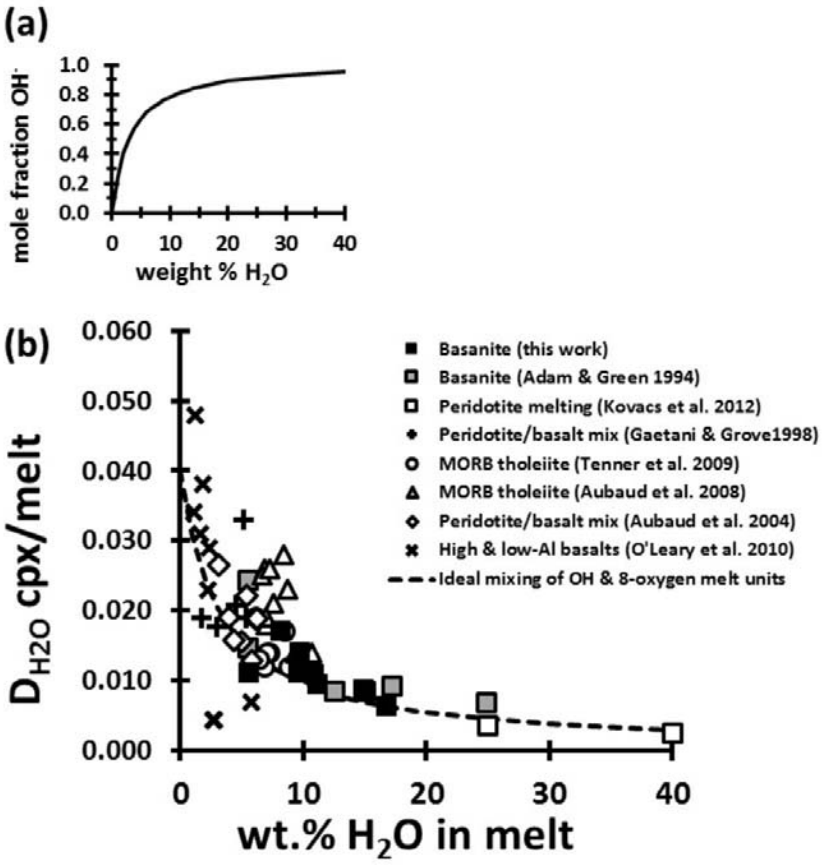
(a)
mole fraction OH
1.0
0.8
0.6
0.4
0.2
0.0
0
10
20
30
40
weight % H2O
(b)
0.060
0.050
0.040
0.030
0.020
0.010
0.000
DH2O cpx/melt
0
10
20
30
40
wt.% H2O in melt
Basanite (this work)
Basanite (Adam & Green 1994)
Peridotite melting (Kovacs et al. 2012)
Peridotite/basalt mix (Gaetani & Grove1998)
MORB tholeiite (Tenner et al. 2009)
MORB tholeiite (Aubaud et al. 2008)
Peridotite/basalt mix (Aubaud et al. 2004)
High & low-Al basalts (O'Leary et al. 2010)
Ideal mixing of OH & 8-oxygen melt units

Fig. 9

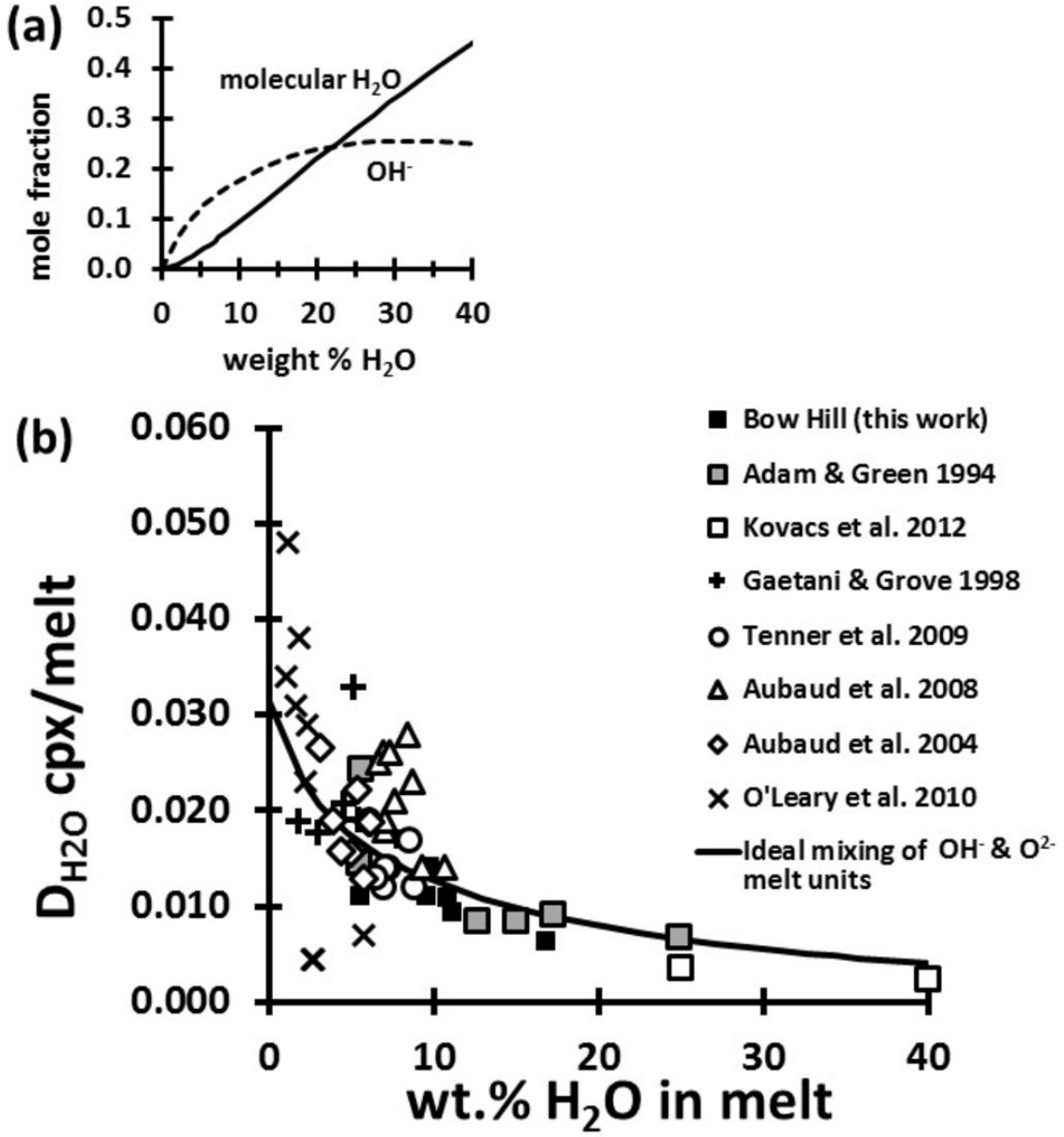
(a)
0.5
0.4
0.3
0.2
0.1
0.0
mole fraction
molecular H_2O
OH^-
0
10
20
30
40
weight % H_2O
(b)
0.060
0.050
0.040
0.030
0.020
0.010
0.000
D_{H2O} cpx/melt
Bow Hill (this work)
Adam & Green 1994
Kovacs et al. 2012
Gaetani & Grove 1998
Tenner et al. 2009
Aubaud et al. 2008
Aubaud et al. 2004
O'Leary et al. 2010
Ideal mixing of OH^- & O^{2-} melt units
0
10
20
30
40
wt.% H_2O in melt

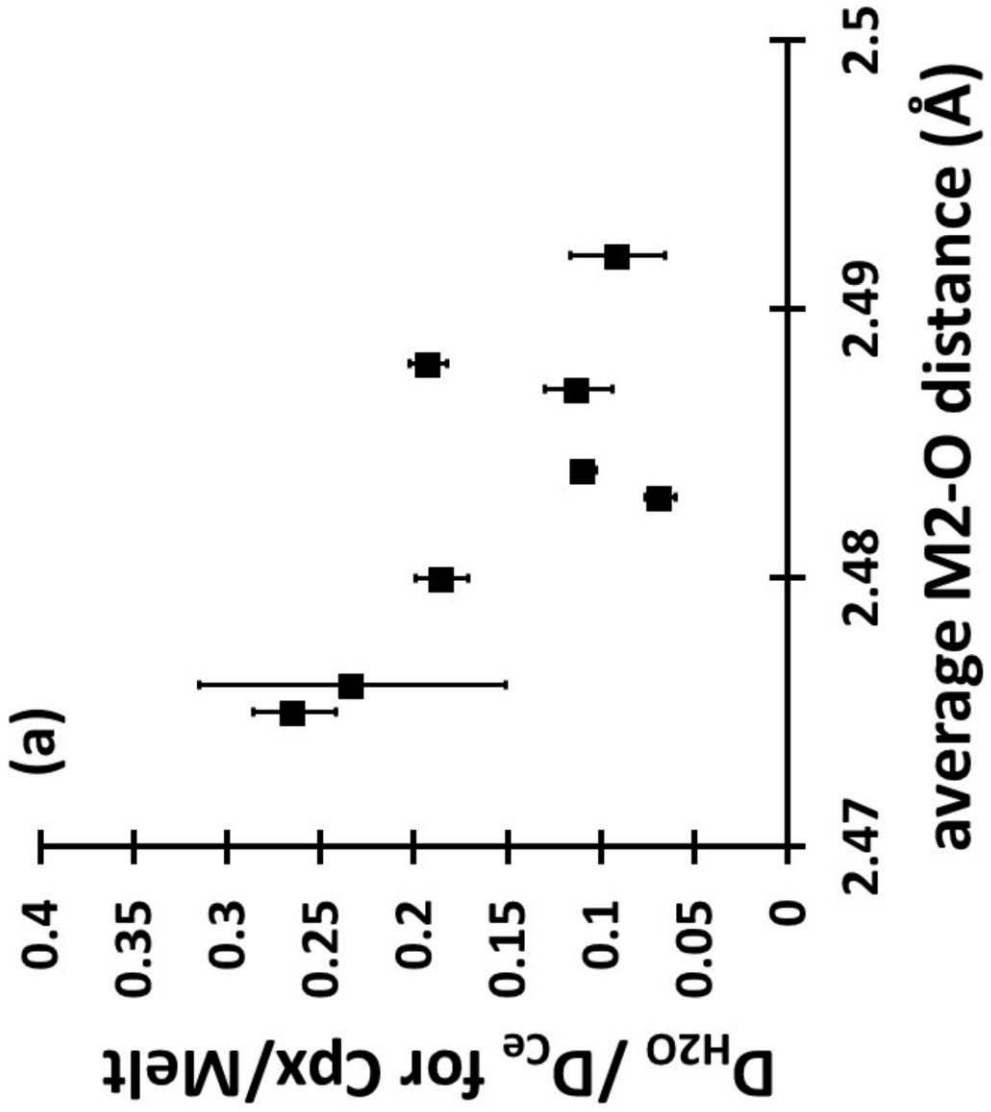
(a)
D_{H2O}/D_{Ce} for Cpx/Melt
0.4
0.35
0.3
0.25
0.2
0.15
0.1
0.05
0
2.47
2.48
2.49
2.5
average M2-O distance (Å)

Fig. 10a

This is a preprint, the final version is subject to change, of the American Mineralogist (MSA)
Cite as Authors (Year) Title. American Mineralogist, in press.
(DOI will not work until issue is live.) DOI: http://dx.doi.org/10.2138/am-2016-5437

Fig. 10b

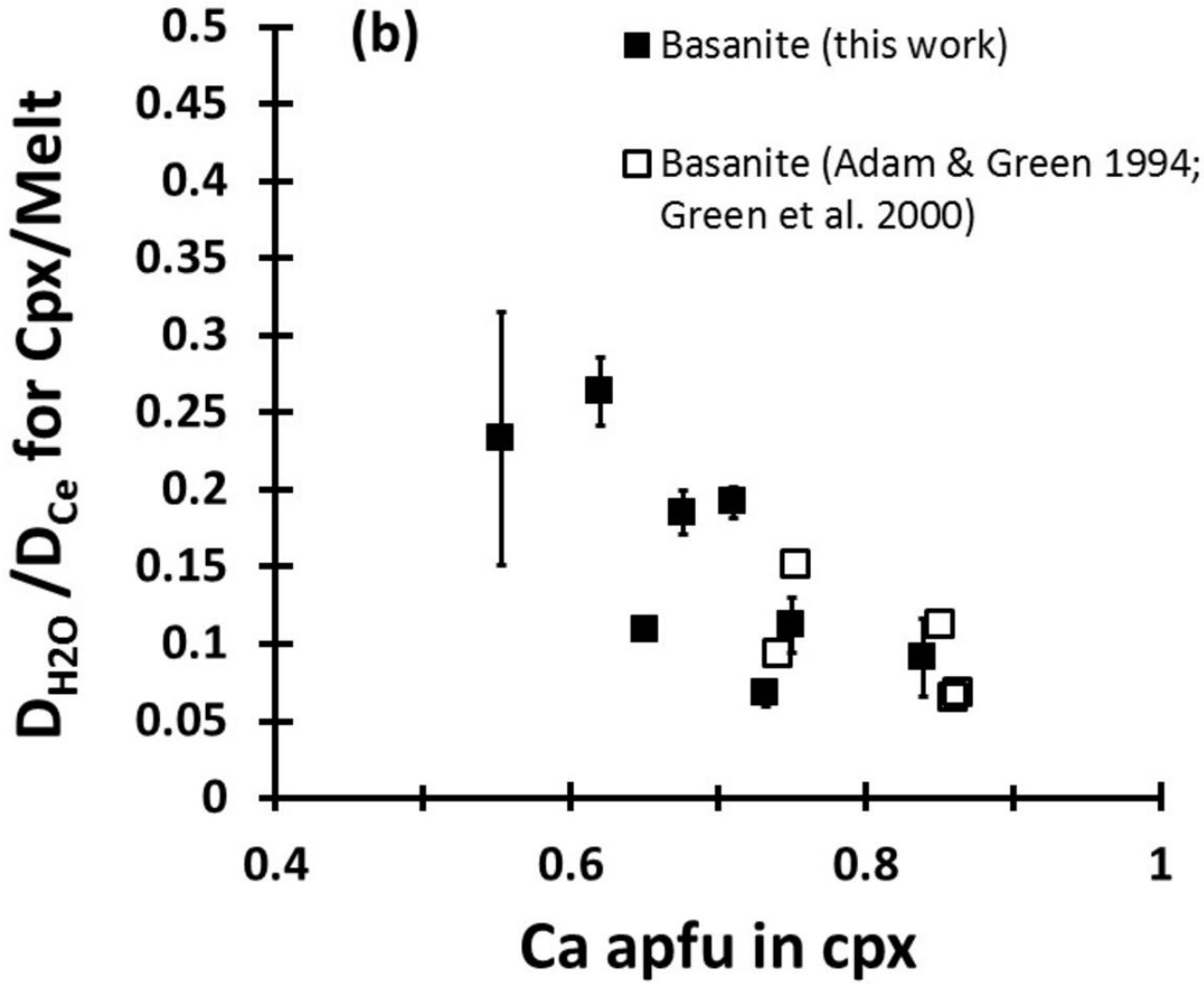

This is a preprint, the final version is subject to change, of the American Mineralogist (MSA)
Cite as Authors (Year) Title. American Mineralogist, in press.
(DOI will not work until issue is live.) DOI: http://dx.doi.org/10.2138/am-2016-5437

Fig. 10c

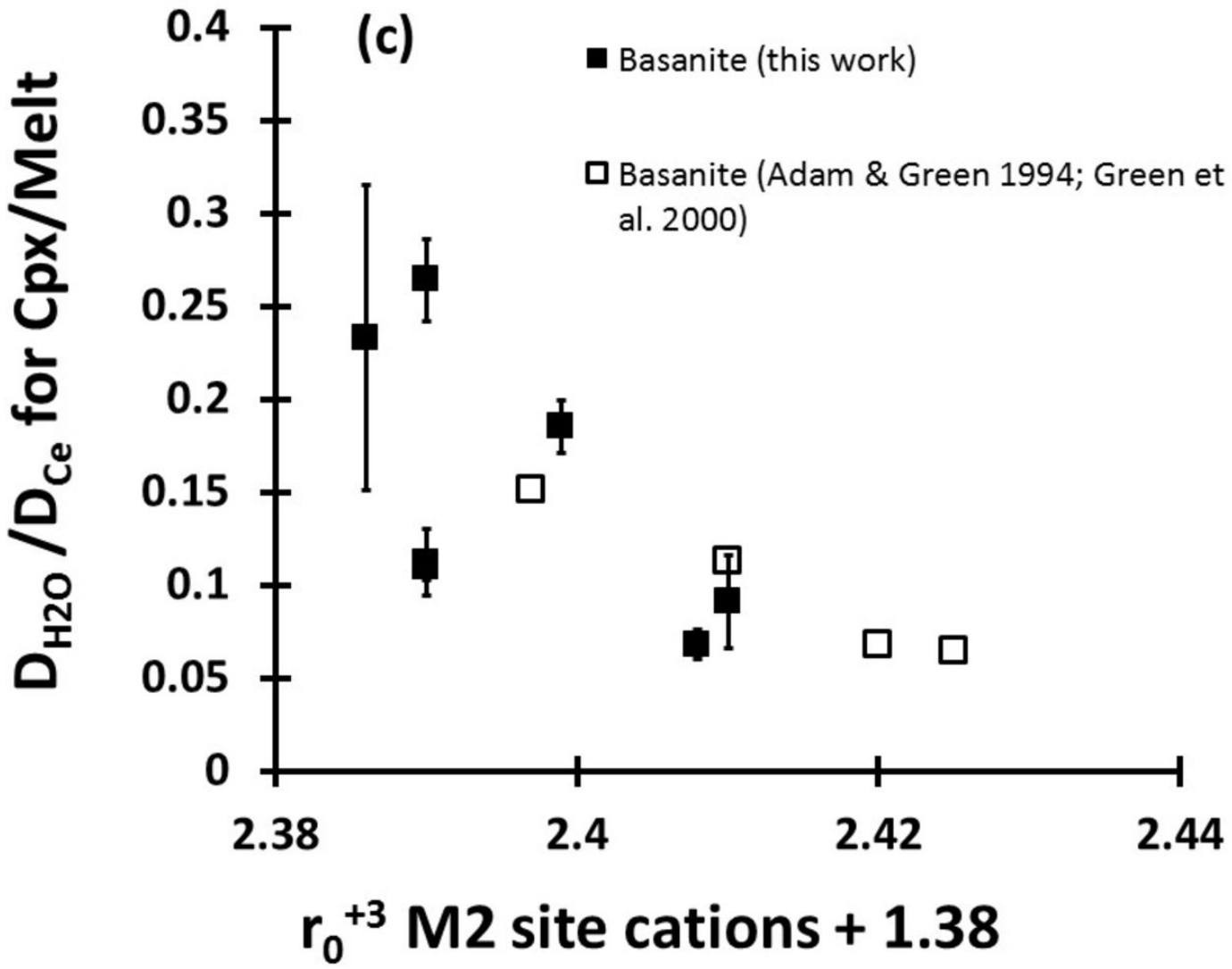

Fig. 11

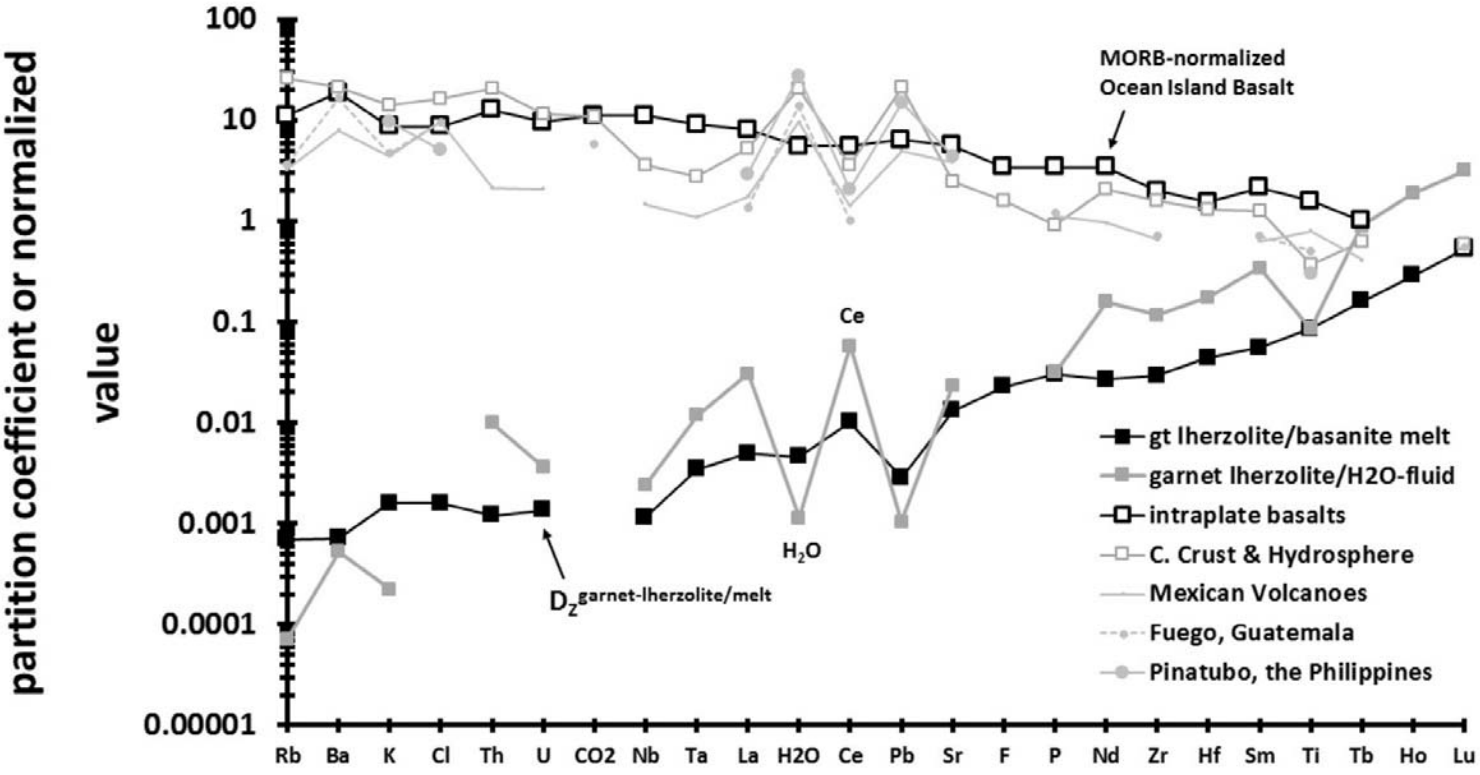
partition coefficient or normalized value
100
10
1
0.1
0.01
0.001
0.0001
0.00001
MORB-normalized
Ocean Island Basalt
Ce
H2O
DZgarnet-lherzolite/melt
gt lherzolite/basanite melt
garnet lherzolite/H2O-fluid
intraplate basalts
C. Crust & Hydrosphere
Mexican Volcanoes
Fuego, Guatemala
Pinatubo, the Philippines
Rb Ba K Cl Th U CO2 Nb Ta La H2O Ce Pb Sr F P Nd Zr Hf Sm Ti Tb Ho Lu

Table1

Experimental conditions and run products for experiments on the Bow Hill nepheline basanite that are described in this study

Run	GPa	°C	Wt. % H_2O in starting mix	Run products
1951	1.0	1025	7.5	4cpx+9ol+18amph+0.1ap+68.9melt
R79	1.0	1075	5.0	4cpx+10ol+86melt
1950	2.0	1050	10.0	9cpx+1opx+7mica+17amph+66melt
R77	2.0	1100	10.0	6cpx+3ol+91melt
R78	2.5	1100	7.5	13cpx+4mica+83melt
1948	2.5	1160	7.5	11cpx+1opx+88melt
R80	3.0	1170	7.5	18cpx+4opx+78melt
1956	3.5	1180	10.0	24gt+12cpx+64melt
1955	3.5	1190	10.0	14gt+7cpx+79melt

Abbreviations include: Wt. %, weight %; gt, garnet; cpx, clinopyroxene; opx, orthopyroxene; ol, olivine; amph, amphibole; ap, apatite
Run product modes were calculated from mass balances with starting materials (see text for method of calculation)

Table 2

SIMS, LAM and electron microprobe analyses of volatiles and P in experimental run products

Run	1956 melt n = 6	1 std	1955 melt n = 6	1 std	R80 melt n = 6	1 std	1948 melt n = 6	1 std	R78 melt n = 6	1 std	R77 melt n = 6	1 std	1950 melt n = 5	1 std	R79 melt n = 5	1 std	1951 melt n = 5	1 std
CO_2															4827	(478)	5527	(111)
H_2O															46800	(200)	75000	(2000)
F															6198	(31)	7563	(203)
P															9301	(98)	11378	(337)
P by LAM															5730	(58)	6636	(88)
S															185	(2)	421	(18)
C															12612	(152)	23171	(1169)
H_2O by mass balance	163000		133000		99000		85000		120000		110000		141000		58000		103000	
H_2O from La	168000	(4000)	109000	(4000)	98000	(2000)	82000	(2000)	96000	(4000)	112000	(2000)	149000	(3000)	56000	(2000)	107000	(3000)
H_2O by difference	135000		135000		104000		80000		125000		74000		120000		66000		86000	
F by EMP	4100	(700)			3500	(500)	3300	(200)	3200	(100)	3000	(200)	2300	(200)	3600	(100)	2600	
Cl by EMP	4600	(900)			6200	(500)	4400	(600)	2700	(600)	4200	(800)	3500	(400)	10800	(200)	14500	(100)

Run	1956 cpx n = 4	1 std	1955 cpx n = 1	1 std	R80 cpx n = 5	1 std	1948 cpx n = 5	1 std	R78 cpx n = 3	1 std	R77 cpx n = 5	1 std	1950 cpx n = 2	1 std	R79 cpx n = 4	1 std	1956 garnet n = 2	1 std
CO_2	8	7	20		16	10	13	7	26	17	347	678	48	24	3	4	8	1
H_2O	1047	41	1191		1375	149	1390	100	1060	58	1045	160	1275	137	608	135	352	66
F	229	15	143		247	15	264	13	187	14	202	20	228	10	326	71	35	0
P	172	35	64		110	47	108	52	57	11	70	33	101	43	75	9	259	9
P by LAM	144	18	n.a.		160	66	64	34	65	0	63	11	459	78	101	12	197	32
S	n.d.		n.d.		n.d.		n.d.		n.d.		1	0	n.d.		n.d.		n.d.	
Cl	2	2	n.d.		20	37	1	1	1	1	7	0	4	3	n.d.		2	0

Run	1955 garnet n = 1	1 std	R80 opx n = 3	1 std	1948 opx n = 2	1 std	1950 opx n = 1	1 std	R77 olivine n = 2	1 std	R79 olivine n = 5	1 std	1950 amph n = 5	1 std	R78 mica n = 4	1 std	1950 mica n = 2	1 std
CO_2	22		13	0	49	45	15		20	14	44	65	150	200	237		425	367
H_2O	216		803	12	1211	45	649		166	4	94	14	16900	300	35100	300	39100	100
F	26		149	42	127	6	82		34	0	19	1	4983	98	8177	143	10423	2
P	254		39	13	27	2	24		265	22	406	98	184	18	11	1	11	1
P by LAM	197	32	n.a.		n.a.		396	67	245	8	310	93	147	12	16	10	32	3
S	n.d.		n.d.		n.d.		n.d.		n.d.		n.d.		5	0	12	0	14	0
Cl	n.d.		1	0	1	1	1		n.d.		n.d.		811	23	1329	36	1436	53
F by EMP													2200	300	3600	200	4400	500
Cl by EMP													700	100	1500	600	1000	100

All concentrations are in ppm unless otherwise indicated.
EMP = electron microprobe. LAM = laser ablation micro-probe and inductively-coupled mass spectrometry (from Adam and Green unpublished data).
m.b. = H_2O concentrations derived from mass balances of run products and starting materials. H_2O from La = H_2O concentrations estimated from La concentrations and known H_2O/La in quenched melts. H_2O by difference is the difference in the analytical totals of all non-aqueous components relative to 100 %. All other analyses were by SIMS. Figures in parentheses are single standard deviations calculated from data for replicate analyses.
n = number of replicate analyses
n.d. = not detected; n.a. = not analysed

Table 3 Mineral/melt partition coefficients for H_2O, F and Cl

run	1956	1955	R80	1948	R78	R77	1950	R79
GPa	3.5	3.5	3.0	2.5	2.5	2.0	2.0	1.0
°C	1190	1180	1170	1160	1100	1100	1050	1075
	cpx	cpx	cpx	cpx	cpx	cpx	cpx	cpx
H_2O	0.0062	0.0109	0.0140	0.017	0.0111	0.0093	0.0086	0.011
1 STD	0.0003	0.0005	0.0015	0.001	0.0008	0.0014	0.0009	0.002
F								0.05
1 STD								0.01
run	1956	1955	R80	1948		R77	1950	R79
GPa	3.5	3.5	3.0	2.5		2.0	2.0	1.0
°C	1190	1180	1170	1160		1100	1050	1075
	garnet	garnet	opx	opx		olivine	opx	olivine
H_2O	0.0021	0.0020	0.0075	0.0113		0.0015	0.0060	0.0009
1 STD	0.0002	0.0001	0.0002	0.0005		0.0001	0.0002	0.0001
F								0.0031
1 STD								0.0002
run					R78		1950	1950
GPa					2.5		2.0	2.0
°C					1100		1050	1050
					mica		mica	amph
H_2O					0.33		0.36	0.194
1 STD					0.01		0.01	0.005
F[1]					2.6		1.9	1.0
1 STD					0.1		0.3	0.2
Cl[1]					0.5		0.29	0.20
1 STD					0.1		0.03	0.02

[1]D values for F and Cl in amphibole and mica are based on electron micro-probe analyses. All other values are based on SIMS data.
H_2O results are based on La concentrations and assumed H_2O/La in melts (presumed equal to H_2O/La in starting mixes).